Identification of new MmpL3 inhibitors by untargeted and targeted mutant screens defines MmpL3 domains with differential resistance

John T. Williams[1], Elizabeth R. Haiderer[1], Garry B. Coulson[1], Kayla N. Conner[1], Edmund Ellsworth[2], Chao Chen[3], Thomas Dick[3], and Robert B. Abramovitch[1*]

[1]Department of Microbiology and Molecular Genetics, and [2]Department of Pharmacology and Toxicology, Michigan State University, East Lansing, Michigan, 48824, United States. [3]Public Health Research Institute, Rutgers New Jersey Medical School, Newark, NJ, 07130, United States.

Corresponding Author

Robert B. Abramovitch

E-mail: abramov5@msu.edu

Phone: (517) 884-5416

Fax: (517) 353-8957

Abstract

The *Mycobacterium tuberculosis* (Mtb) mycolic acid flippase MmpL3 has been the proposed target for multiple inhibitors with diverse chemical scaffolds. This diversity in chemical scaffolds has made it difficult to predict compounds that inhibit MmpL3 without whole genome sequencing of isolated resistant mutants. Here we describe the identification of four new inhibitors that select for resistance mutations in *mmpL3.* Using these resistant mutants, we conducted a targeted whole-cell phenotypic screen of 163 novel Mtb growth inhibitors for differential growth inhibition of wild type Mtb as compared to a pool of twenty-four unique *mmpL3* mutants. The screen successfully identified six additional putative MmpL3 inhibitors. The compounds were bactericidal both *in vitro* and against intracellular Mtb. Mtb cells treated with these compounds were shown to accumulate trehalose monomycolate and have reduced levels of trehalose dimycolate, supporting MmpL3 as the target. The inhibitors were mycobacteria specific with several also showing activity against the non-tuberculosis mycobacterial species *M. abscessus.* Cluster analysis of cross resistance profiles generated by dose response experiments for each combination of 13 MmpL3 inhibitors against each of the 24 *mmpL3* mutants defined two clades of inhibitors and two clades of *mmpL3* mutants. Pairwise combination studies of the inhibitors revealed interactions that were specific to the clades identified in the cross-resistance profiling. Additionally, modeling of resistance substitutions to the MmpL3 crystal structure revealed clade specific localization of the residues to specific domains of MmpL3, with the clades showing differential resistance. Several compounds exhibited high solubility and stability in microsomes and low cytotoxicity in macrophages, supporting their further development. The combined study of multiple mutants and novel compounds provides new insights into structure-function interactions of MmpL3 and small molecule inhibitors.

Introduction

In efforts to identify new tuberculosis (TB) antibiotics, whole cell-based phenotypic screens have been conducted against the pathogen *Mycobacterium tuberculosis* (Mtb). Over the last decade, several of these screens have identified MmpL3 as the proposed target for diverse small molecule inhibitors including AU1235, BM212, C215, DA-5, E11, indolecarboxamides, HC2091, NITD-349, PIPD1, Rimonabant, Spiro, TBL-140, THPP and SQ109[1, 2, 3, 4, 5, 6, 7, 8, 9, 10, 11, 12]. MmpL3 is an essential flippase responsible for transporting acetylated-trehalose monomycolate (TMM) synthesized in the cytoplasm to the pseudo-periplasmic space[13, 14, 15, 16, 17]. These TMMs are then converted into trehalose dimycolate (TDM) by the Ag85 complex in the cell envelope [18]. MmpL3 is essential as evidenced by a pre-existing rescue allele being required to generate an *mmpL3* knockout[2, 14, 17, 19, 20, 21], lack of mutants in high-throughput transposon mutagenesis screens[22, 23], and studies that show rapid killing *in vitro* and *in vivo* in acute infection models when *mmpL3* expression is conditionally inhibited[14, 19]. This makes MmpL3 an attractive target for drug development, with one of its inhibitors, SQ109, currently in clinical trials [24].

MmpL3 inhibitors fall into diverse classes of chemical scaffolds [25, 26, 27], making it hard to computationally predict potential MmpL3 inhibitors based on chemical scaffolds. However, given the frequent finding of MmpL3 as a target, it is reasonable to expect that many new hits in a high throughput screen (HTS) may be acting against MmpL3. MmpL3 inhibitors have been identified by the isolation and sequencing of resistant mutants with single nucleotide variations (SNVs) mapping to the coding region of *mmpL3,* which is time-consuming and costly. Efforts to discover MmpL3 inhibitors using targeted approaches include generating hypomorphs, where a *mmpL3* knock down strain showed enhanced sensitivity to MmpL3 inhibitors, including AU1235 [14]. However, this strain was also shown to be sensitive to isoniazid (INH) an inhibitor of InhA of the FAS-II pathway involved in mycolic acid synthesis, suggesting that while a *mmpL3*

knockdown strain has robust screening potential for inhibitors of mycolic acid synthesis, maturation, and transport, such strains are not specific enough to identify inhibitors that selectively target MmpL3.

An alternative approach, employed in this study, is to use a pool of *mmpL3* resistant mutants to discover potential MmpL3 inhibitors. MmpL3 is a member of the resistance nodulation and division (RND) family of proteins, normally associated with efflux pumps in gram-negative bacteria [2, 13, 17]. However, evidence suggests MmpL3 does not act as a general efflux pump in resistant backgrounds as resistant mutants do not differ in the amount of inhibitor isolated from cell fractions compared to WT Mtb [2]. In further support that MmpL3 does not act as an efflux pump, the low level of cross resistance to compounds not associated with MmpL3 inhibition, including INH, suggests that MmpL3 does not act as a general efflux pump [21]. This suggests that MmpL3 inhibitor resistant mutants could be used to screen for other potential MmpL3 inhibitors. The goal of this study was to discover MmpL3 inhibitors from a collection of 163 newly discovered, uncharacterized inhibitors of Mtb growth [28]. Herein we describe the identification of four novel MmpL3 inhibitors by isolation of resistant Mtb mutants with mutations mapping to *mmpL3.* These twenty-four unique Mtb *mmpL3* mutant strains were then pooled into a single batch culture to conduct a targeted whole-cell phenotypic screen to identify six new scaffolds with reduced activity in the mixed mutant population as compared to the wild type. Cross resistance and compound interactions studies demonstrate specific structure function interactions between the molecules and MmpL3 and defined domains of MmpL3 associated with differential resistance to MmpL3 inhibitors.

Results

Identification of four new MmpL3 inhibitors by isolation of resistant mutants

Previously, two HTS were conducted, targeting the two component regulatory systems, DosRST and PhoPR[28, 29, 30]. In addition to inhibitors targeting these pathways, a series of compounds was identified that inhibited Mtb growth independent of the targeted pathways [9, 28, 30]. A series of high throughput assays were then conducted to prioritize these compounds (Supplemental Figure 1) including confirming hits, testing for eukaryotic cytotoxicity in primary murine bone marrow-derived macrophages (BMMΦ, ≤10% cytotoxicity), and testing for the ability of the compounds to inhibit Mtb growth inside BMMΦ (≥25% growth inhibition). Results of these screens identified 216 compounds of which 163 commercially available compounds were purchased as fresh powders. In order to identify the mechanism of action of these Mtb growth inhibitors our lab selected several compounds with potent Mtb growth inhibition, both *in vitro* and in macrophages, as well as low eukaryotic cytotoxicity.

Four compounds of interest HC2060, HC2149, HC2169, and HC2184 (1-({1-[4-(Benzyloxy)-3-methoxybenzyl]piperidin-3-yl)carbonyl}azepane, N-[2-Methyl-6-(trifluoromethyl)pyridin-3-yl]-4-(trifluoromethyl)benzamide, Ethyl 3-{[(3,4-dihydro-2H-chromen-3-ylamino)carbonyl]amino}benzoate, and N-(2-Diethylaminoethyl)-N-(5,7-dimethyl-1,3-benzothiazol-2-yl)furan-2-carboxamide, respectively) (Figure 1a) had half maximal effective concentrations (EC_{50}) ranging from 1.8 μM to 16.9 μM *in vitro* (Figure 1b, Table 1). All four compounds had bactericidal activity when measured at 20 μM (2x the initial screening concentration) (Figure 1c). To our knowledge, the structures of these compounds are unique from previously described inhibitors of Mtb growth.

To understand the mechanism of action of these four compounds, resistant mutants were isolated using solid agar plates (7H10 OADC) amended with 20 or 40 μM of each compound inoculated with 10^9 CFU of Mtb (Erdman). Isolated mutants were tested for

123 resistance via dose response curves. Confirmed resistant clones were isolated as single
124 colonies and retested to confirm resistance (Supplemental Figure 2a-d). Genomic DNA was
125 extracted from confirmed resistant mutant strains and the genomes were sequenced. Analysis
126 of the genome sequences identified single nucleotide variants (SNVs) in all of the genomes in
127 the coding region of *mmpL3* (Rv0206c, Supplemental Table 1). These mutations encoded for
128 nonsynonymous mutations located throughout the gene (Supplemental Table 1, Supplemental
129 Figure 2e). These findings suggest these compounds may be functioning as MmpL3 inhibitors.
130

131 **Modulation of TMM and TDM accumulation**

132 MmpL3 is responsible for the transport of TMM across the inner membrane [14, 15, 16, 18]. To
133 determine if these compounds inhibited the activity of MmpL3, cultures of Mtb were grown in the
134 presence of ^{14}C-acetate and treated for 24 h with 20 μM of HC2060, HC2149, HC2169,
135 HC2184, SQ109 or equal volumes of dimethylsulfoxide (DMSO). Radiolabeled lipids were
136 isolated and analyzed by thin layer chromatography (TLC) (Figure 2a, Supplemental Figure 3a).
137 The results of the lipid assay show that TMM accumulates in Mtb samples treated with the
138 proposed MmpL3 inhibitors as well as the SQ109 treated samples. Additionally, TDM
139 significantly decreased in cultures treated with HC2169 and HC2184 as well as the positive
140 control SQ109 (Figure 2a and Supplemental Figure 3a). These results are consistent with
141 previously described MmpL3 inhibitors [1, 2, 3, 4, 6, 7, 8, 9, 26] and support that these four compounds
142 inhibit MmpL3 activity.
143

144 **Targeted whole cell phenotypic screen for MmpL3 Inhibitors**

145 The identification of four new MmpL3 inhibitors, as well as the previously published
146 inhibitor HC2091 (6), suggested additional MmpL3 inhibitors may exist in the prioritized 163-
147 compound library of Mtb growth inhibitors (Supplemental Figure 1). Review of the known
148 MmpL3 inhibitor scaffolds and those in our compound library identified HC2172 as the

previously described MmpL3 inhibitor C215 [7]. A recent study by McNeil *et al.,* showed that *mmpL3* mutant strains had low cross resistance against non-MmpL3 inhibitors[21], suggesting that *mmpL3* mutants could be used to screen for MmpL3 inhibitors. Additionally, this study also showed that different mutations conferred varying levels of cross resistance between MmpL3 inhibitors. We therefore hypothesized that by pooling unique *mmpL3* mutant strains into a single mixed culture we could overcome limitations of cross resistance variability. For the targeted phenotypic screen, we directly compared percent growth inhibition (%GI) of either WT or a mixed *mmpL3* mutant pool consisting of twenty-four unique *mmpL3* mutant strains, including three strains previously described as resistant to HC2091 [9] (see Supplemental Table 2). The cultures were treated with 20μM of each of the 163-Mtb growth inhibitors as well as DMSO (negative control), Rifampin (RIF, positive control), Bedaquiline (BDQ), Clofazimine (CFZ), INH, para-aminosalicylic acid (PAS), H_2O_2, or SQ109 for a total of 171 different treatments (Supplemental Figure 4a and 4b). The results of this screen identified thirty-two compounds with 15% GI in the WT background and 1.5x reduced activity in the mixed *mmpL3* mutant background relative to the WT background (examples of positive hits are illustrated in red in Figure 3a). These hits were tested by dose response experiments conducted in both the WT and mixed *mmpL3* mutant background. In total, we identified thirteen compounds with reduced activity in the mixed *mmpL3* mutant background (Table 1, Supplemental Figure 5). Included in our confirmed hits were each of the five inhibitors used to generate the *mmpL3* mutant strains (HC2060, HC2091, HC2149, HC2169, and HC2184) and the two control compounds C215 and SQ109. The targeted screen also identified six novel inhibitors including HC2032, HC2099, HC2134, HC2138, HC2178, and HC2183 (ethyl 4-[(2E)-2-(4,7,7-trimethyl-3-oxo-2-bicyclo[2.2.1]heptanylidene)hydrazinyl]benzoate, 2-[(6-chloro-1H-benzimidazol-2-yl)sulfanyl]-N,N-di(propan-2-yl)acetamide, N-(2-methoxy-5-nitrophenyl)-1-oxo-4-phenylisochromene-3-carboxamide, 1-cyclohexyl-3-[4-[(2-fluorophenyl)methyl]-3-oxo-1,4-benzoxazin-7-yl]urea, 1-cyclooctyl-4-(2,5-dimethylphenyl)piperazine, and 2-[(6-methyl-1H-benzimidazol-2-yl)sulfanyl]-

N,N-di(propan-2-yl)acetamide, respectively) (Figure 3b), which have not been previously described as MmpL3 inhibitors. The amount of resistance conferred by the mixed *mmpL3* mutant strains against each compound varied, with some compounds, like HC2032, HC2138, and HC2169 losing nearly all activity in the mutant background (Supplemental Figure 5) as indicated by the high Relative EC_{50} (fold difference between *mmpL3* mutant pool and WT) values of >36, >20, and >44 (Table 1). Despite the high activity of SQ109 in the WT background, the relative EC_{50} was only 2 (Table 1); however, this observation is consistent with previous studies which only report marginal increases in MIC values in *mmpL3* mutant backgrounds [8, 9, 21, 26]. Included in our hits were two urea-based compounds HC2138 and HC2169 (Figure 1 and Figure 3b). These urea-based compounds have structures reminiscent of the adamantyl-urea MmpL3 inhibitor AU1235 [2]. Additionally, two of the compounds identified in the screen HC2099 and HC2183 had high structure similarity.

The compounds were also tested for eukaryotic cytotoxicity, solubility and stability in mouse microsomes, and the structures were confirmed by mass spectrometry (Table 1). The compounds exhibited low cytotoxicity (>100μM), consistent with our secondary assay screening. Compounds exhibited varying levels of solubility with HC2169 and HC2138 showing lower solubility (66μM and 17μM respectively) but high microsome stability (122% and 168% respectively), and compounds like HC2183 showing high solubility (>200μM) but low microsome stability (25%). Interestingly HC2099, which has high structure similarity to HC2183 showed higher solubility (178μM) and higher microsome stability (71%). Several of the compounds (e.g. HC2091, HC2099, HC2138 and HC2149), exhibited favorable solubility and microsome stability, with no observed macrophage cytotoxicity, supporting their potential for further development.

The phenotypic screen was selective as it did not identify any of the control treatments known to not target MmpL3 including BDQ, INH, PAS, H_2O_2, or HC2051, a proposed Pks13 inhibitor (given its similarity to the TAM16 [31, 32]). To confirm the specificity of our screen, we conducted dose response studies in both the WT and mixed *mmpL3* mutant background for

each of the aforementioned inhibitors, as well as RIF. Results of the dose response studies did not identify any significant levels of resistance to these compounds in the mixed *mmpL3* mutant background (Supplemental Table 3, Supplemental Figure 6). This was true for both inhibitors of mycolic acid synthesis and maturation (INH and HC2051), suggesting our screen was specific for inhibitors of MmpL3. Consistent with previous results, we identified increased susceptibility to RIF treatment in the mixed *mmpL3* mutant background[21] (Supplemental Table 3, Supplemental Figure 6). The dose response profiles for BDQ, CFZ, and PAS did not show any differences in susceptibility, further supporting that *mmpL3* mutations do not confer resistance through general efflux.

Modulation of TDM, membrane potential and viability

To determine if the six compounds identified in the screen can inhibit MmpL3 activity, we examined accumulation of TMM and TDM as described above. The inhibitors modulated mycolic acid accumulation in whole cell extracts, with lipids for all treatments showing a significant accumulation in TMM (except for HC2134) and treatment with HC2032, HC2099, HC2138, and HC2178 showing a significant decrease in TDM relative to the DMSO control samples (Figure 2b and 2c, Supplemental Figure 3b). A recent report has shown that because MmpL3 activity is dependent on the proton motive force (PMF), disruptors of PMF, such as the protonophore carbonyl cyanide m-chlorophenyl hydrazine (CCCP) can also modulate MmpL3 activity [26]. Studies have suggested that some proposed MmpL3 inhibitors such as SQ109 and E11 may indirectly target MmpL3 through disruption of the membrane potential [6, 15, 26]. To determine if the newly identified inhibitors disrupt membrane potential ($\Delta\psi$) we conducted dose response studies using a $DiOC_2$-based assay. Some compounds, including HC2060, HC2169, and HC2183 did not disrupt membrane potential (Table 1, Supplemental Figure 7), while others, such as HC2032, HC2099, HC2134, HC2138, HC2149, HC2178, HC2184 and C215 did disrupt membrane potential (Table 1, Supplemental Figure 7). Consistent with previous observations

HC2091 did not disrupt membrane potential, while SQ109 did disrupt membrane potential (Table 1, Supplemental Figure 7) [9, 15, 26]. Surprisingly, there were differences in outcome for the two urea containing compounds HC2169 and HC2138 as well as between HC2099 and HC2183 which only differ by a chloro and methyl substitution, respectively. The results for HC2138 and HC2169 is also interesting because the previously described urea-based MmpL3 inhibitor, AU1235, does not disrupt the membrane potential[15, 26]. These results suggest that the ability to disrupt membrane potential is highly structure specific.

Because MmpL3 is essential for viability of replicating bacteria, we tested these compounds for bactericidal activity using a firefly luciferase (*luc*) reporter strain of Mtb in conjunction with a luciferase assay. This assay relies on active luciferase generated by the reporter Mtb strain, and the presence of ATP which is generated in living cells, but rapidly hydrolyzed in lysed cells. All of these compounds showed bactericidal activity (Supplemental Figure 8). These results suggest that the growth inhibition is due to compounds killing Mtb in a dose dependent manner. The bactericidal activity of these inhibitors is consistent with these compounds targeting MmpL3 which is essential for cell viability [14, 19].

Spectrum of activity

While MmpL3 is conserved in mycobacteria, functional orthologs are not found in other bacteria and fungi. Despite this, several proposed MmpL3 inhibitors including BM212, THPP, and SQ109 have been shown to inhibit multiple bacterial and fungal species [8, 33, 34, 35] while other MmpL3 inhibitors including HC2091, AU1235, and indolecarboxamides are specific to mycobacteria. To define the spectrum of activity, the compounds were tested against several diverse species including *Staphylococcus aureus, E. coli, Pseudomonas aeruginosa, Proteus vulgaris,* and *Enterococcus faecalis* (Table 2). For HC2032, HC2060, HC2099, HC2149, HC2169, HC2178 and HC2184, even at high concentrations (200μM), no inhibition was observed against non-mycobacteria. However, these inhibitors were positive for activity against

253 other mycobacteria, including the pathogenic non-tuberculosis species *M. abscessus* and the
254 saprophytic species *M. smegmatis* (Table 2). For example, HC2091, HC2099, and HC2134
255 exhibited MIC_{50} of 6.25 μM, 25 μM and 12.5 μM against *M. abscessus,* respectively.
256 Additionally, all of the MmpL3 inhibitors tested, except for HC2149, were active against *M.*
257 *smegmatis*. This suggests that most of the inhibitors are specific for mycobacteria and may be
258 effective against diverse mycobacterial species. The observation that HC2134 and C215 are
259 active against non-mycobacterial species has been observed with other MmpL3 inhibitors [24, 34,
260 35] and may be due to a non-specific activities such as PMF disruption.
261
262 **Activity against intracellular Mtb**
263 The compounds were tested against Mtb growing in BMMΦ using a luciferase
264 expressing Mtb strain. BMMΦ were infected with Mtb and treated with the inhibitors for six days
265 across a range of concentrations (200 – 0.3μM). The BMMΦ EC_{50} values are summarized in
266 Table 1 and Supplemental Figure 9. The results of the assay show that many of the inhibitors
267 have bactericidal activity in MΦ several magnitudes lower than the eukaryotic cytotoxicity CC_{50},
268 supporting a high selectivity index. The identification of bactericidal effects against Mtb in
269 BMMΦ is consistent with genetic knockdown studies that show *mmpL3* is essential for actively
270 replicating bacteria (4,5).
271
272 **Cross resistance profiles indicate specific MmpL3 protein-inhibitor interactions**
273 While the results of the screen showed potential for rapid identification of MmpL3
274 inhibitors, the screen relied on the use of a mixed mutant population. To resolve this issue, we
275 conducted dose response studies for each combination of the twenty-four unique *mmpL3*
276 mutants against each MmpL3 inhibitor identified from the screen (with WT Mtb as a control).
277 Because there was a complete lack of activity for compounds like HC2169 against HC2169-
278 specific resistant mutants (Supplemental Figure 2c), units of measure such as EC_{50} and MIC

cannot be calculated, or are not a good measure for comparing responses. Instead, we used the area under the curve (AUC) for each dose response in the *mmpL3* mutant backgrounds relative to the AUC for the WT response for a given treatment (Supplemental Table 4). Because the compounds have differences in potency, the AUC for the WT for each treatment differs and to account for this issue we normalized our values by Z-score for each treatment[36]. Cluster analysis grouped the data based on both treatment effectiveness and resistance conferred by each *mmpL3* mutant. The resulting cluster-gram (Figure 4) shows that both compounds and *mmpL3* mutant strains, denoted by the amino acid substitutions, fall into distinct clades. The compounds fall into two distinct clades, Clade A (Red), which contains HC2134, HC2138, HC2149, HC2169, and Clade B (Green) which contains HC2032, HC2060, HC2091, HC2099, HC2178, HC2183, HC2184, C215, and SQ109. The identification of two distinct clades of compounds, suggested that the compounds may be interacting with the MmpL3 protein in distinct ways.

The resistance mutations also showed specific clustering. Cluster analysis of the strains showed that WT clustered on its own and the mutants formed a large complex cluster. Within this large cluster, the *mmpL3* mutant strains formed into two sub-clades; Clade I (Green) which conferred relatively high resistance (lower inhibitor effectiveness) and Clade II (Red) which conferred relatively low resistance (higher inhibitor effectiveness). Clade I, which contained eleven *mmpL3* mutant strains denoted as Y252C, V285G, G253E, L567P, I585S, S591I, S591T, V643M, F644N, F644L, and M649L. Clade II consisted of the remaining thirteen *mmpL3* mutant strains denoted as Q40H, V240A, I244T, L299Q, T311I, R373W, M649T, A662E, T670L, L693P, M695T, L699M, and A700T. Surprisingly M649T fell into Clade II mutations, this was striking as the *mmpL3* mutant denoted as M649L was clustered with the Clade I *mmpL3* strains.

304

305 **Pairwise Combination Studies using DiaMOND**

306 We hypothesized that the clustering of compounds into two clades was due to their
307 having distinct interactions with MmpL3; therefore, combination treatments may reveal
308 antagonistic, additive or synergistic interactions. In order to test this hypothesis in whole cell
309 Mtb, we used the recently described diagonal measurement of *n*-way drug interactions
310 (DiaMOND) approach [37]. RIF was included as a control for these assays, as this drug has been
311 shown to be synergistic when tested with other MmpL3 inhibitors such as AU1235 and SQ109
312 [38, 39]. The results of DiaMOND, shown in Figure 5, identified synergistic interactions ($FIC_2 < 1.0$)
313 between all combinations of MmpL3 inhibitors and RIF. Additionally, the results identified mostly
314 additive interactions ($FIC_2 = 1.0$) consistent with the compounds sharing a single target.
315 Interestingly, all combinations between MmpL3 inhibitors and the compounds HC2134,
316 HC2138, HC2149, and HC2169 showed antagonistic interactions ($FIC_2 > 1.0$). These four
317 compounds were clustered together in Clade A in the cross-resistance profiles described above
318 (Figure 4). This antagonistic relationship further supports that the Clade A compounds are
319 distinct from the Clade B compounds. Another observation from the DiaMOND assay is that
320 pairwise combinations of compounds HC2060, C215, and SQ109 all had synergistic interactions
321 (Figure 5). The reason for this observation is not clear as the compounds did not have
322 differential cross resistance profiles (Figure 4). Interestingly, combinations of HC2060 and
323 C215, but not SQ109, with the Clade A compounds HC2139 and HC2169 did not reveal
324 antagonist interactions, but instead additive interactions (Figure 5). This finding supports that
325 these HC2060 and C215 compounds interact with MmpL3 in a manner distinct from the other
326 compounds.

327

328

Discussion

The cross-resistance profiles showed that the *mmpL3* mutant strains clustered separately into two clades, Clade I and Clade II, with WT clustering on its own as an outgroup (Figure 4). Recently, the crystal structure of *M. smegmatis* MmpL3 has been solved by two independent groups[12, 40]. In order to understand this observation, we generated a 3D model of the Mtb MmpL3 protein aligned to the *M. smegmatis* MmpL3 structure[41] (C-score 0.17, RMSD 8.4 ±4.5Å). Substitutions from the *mmpL3* mutant strains used in the cross-resistance profiles are highlighted in the model (red, green, and blue) (Figure 6). Consistent with previously described resistant strains of Mtb, the majority of the substitutions, localized along the central vestibule with the exception of T670, R373, and A662 which did not align along the central vestibule of the model (Figure 6)[17]. This vestibule is conserved amongst the RND family of proteins and is responsible for the proton translocation that drives protein activity [17, 26]. To understand the clustering pattern of the cross-resistance profiling we highlighted the mutations based on their clade, revealing that the two distinct clades separated spatially in the model. The substitutions of Clade I (Green), that conferred higher resistance, localized towards the cytoplasmic face of the protein. While substitutions of Clade II (Red), which generated lower resistance, localized into two separate locations: i) towards the pseudo-periplasmic face of the protein; and, ii) another region which does not line the central vestibule (Figure 6). Structure function profiling by Belardinelli and colleagues [17] had previously described seven essential residues for MmpL3 function (D251, S288, G543, D640, Y641, D710, and R715) that clustered in a single domain [17]. This study also modeled substitutions commonly identified from resistant mutants to multiple inhibitors to this same region. To determine if the two clades separated based on their approximation to this essential region, we highlighted these seven residues in the model (Supplemental Figure 10). Notably, the two clades separate based on their proximity to these residues, with Clade I substitutions localizing in the same region as the essential residues

and Clade II substitutions localizing distally from the essential residues. This finding suggests that the strength of resistance conferred by a mutation is dependent on the proximity of the substitution to residues essential for MmpL3 function.

Genome sequences of the isolated resistant mutants identified a total of 21 unique mutations in *mmpL3*. These mutations translated to substitutions that were a mix of ones previously described and novel to this study. Included in this list were substitutions that had previously been described including G253E, Y252C, L567P, S591I, V643M, F644L, L699M [1, 2, 5, 6, 8, 9, 21, 31]. Mutations that were unique to this study included ones in positions in V240, I244, V285, L299, T311, R373, I585, A662, and L693. We also isolated mutations that had previously been described to occur in positions Q40, Y252, G253, L567, S591, F644, M649, and L699 [1, 2, 5, 6, 8, 9, 21, 31]. However, the exact substitutions in several of these strains' positions including Q40H, S591T, F644N, and M649T were unique to this study. Our cross-resistance profiling found that G253E, V285G, S591I, S591T, L699M, and A700T, conferred pan resistance including against SQ109. That the number of compounds proposed to target MmpL3 and the large number of substitutions that confer resistance highlights the importance of identifying combinations of drugs that would reduce the frequency of resistance.

The favorable properties of many of these compounds, including low cytotoxicity, high solubility and microsome stability, and activity in macrophages, suggests that these compounds warrant further development as new therapeutics. It is also possible that combinations of these scaffolds may be developed in a single molecule that can function to reduce the frequency of resistance. Three of the compounds used to isolate resistant mutants in this study, HC2149, HC2169 and HC2184, had a frequency of resistance (FoR) of 3×10^{-7}, which is similar to the FoR of other MmpL3 inhibitors that have a FoR ranging from 10^{-7} to 10^{-8} [2, 3, 4, 5, 6, 21]. That the FoR for HC2184 was the same as the FoR for HC2149 and HC2169 is interesting as the cross-resistance profiles and results of DiaMOND analysis suggested that these compounds interact

379 differently with MmpL3. While the antagonistic interactions identified by DiaMOND suggest that
380 scaffold combinations may lower the activity of a single inhibitor, antagonistic drug combinations
381 have been proposed to decrease the rate of resistance [42, 43]. It therefore may be possible to
382 design a single inhibitor that fuses more than one scaffold to decrease the rate of resistance.
383 This hypothesis could initially be tested by conducting pairwise combination studies examining
384 for synergistic reductions in the FoR. Given the relative ease of resistance occurring to MmpL3
385 inhibitors, a reduced FoR could be a valuable new property for this class of inhibitors.

386 Over the past decade, many MmpL3 inhibitor of various chemical scaffolds have been
387 described. The proposed target of these inhibitors has been driven by the mapping of resistance
388 mutations to *mmpL3*. The screening platform we describe here greatly accelerates target
389 identification of such inhibitors. The use of a diverse pool of unique *mmpL3* mutants, rapidly
390 identified inhibitors of MmpL3 activity, as demonstrated by their ability to modulate TDM and
391 TMM accumulation. A subset of these inhibitors was shown to disrupt membrane potential, and
392 potentially the PMF which energizes MmpL3 activity. Two recent studies have suggested that
393 two MmpL3 inhibitors, SQ109 and E11, indirectly inhibit MmpL3 by targeting the PMF despite
394 the isolation of *mmpL3* resistant mutants [6, 15] and co-crystallization of SQ109 to MmpL3[12]. It is
395 therefore possible that some of these new compounds inhibit MmpL3 indirectly by dissipation of
396 the PMF. Notably, the narrow spectrum of activity of most of the isolated compounds for
397 mycobacteria supports that the target is mycobacterium specific, and not a general target that
398 when bound dissipates PMF.

399

400

401 **Methods**

402 **Media and Growth Conditions**

403 Unless otherwise specified, streptomycin resistant strains of Mtb Erdman or CDC1551
404 were cultured in 7H9 media supplemented with 10% OADC (v/v) with 0.05% Tween-80 (v/v) in
405 standing T25, T75 or T150 flasks at 37 ºC with 5% CO_2. Spectrum of activity studies in different
406 bacterial species (Table 2) were conducted as described by Coulson et al., [30], with the
407 exception of the *M. abscessus* studies which are described in the supplemental methods.
408
409 **Dose Response Curves**

410 Mtb was grown in rich medium to an OD_{600} of 0.5-1.0. Cultures were diluted to an OD_{600}
411 of 0.1 in 7H9 medium and aliquoted into black walled clear bottom 96 well assay plates.
412 Compounds were tested between 80-0.13 µM with 2.5-fold dilutions, controls included DMSO
413 and 3 µM RIF. Plates were placed in zip lock bags with moistened paper towels and incubated
414 at 37ºC for 6 days. Plates were read on a PerkinElmer Enspire plate reader. %GI was
415 calculated using DMSO and RIF as 0% and 100% inhibition, respectively. Dose responses were
416 conducted in biological triplicate and repeated at least once. Significant differences of EC_{50} were
417 compared using 95% confidence intervals.

418 To examine the spectrum of activity of the MmpL3 inhibitors, the EC_{50} of each compound
419 was also determined for *M. smegmatis* and other nonmycobacteria, including *S. aureus, E. coli,*
420 *P. aeruginosa, P. vulgaris,* and *E. faecalis*. Tests were performed in 96-well plates in LB broth
421 with shaking at 37°C, with the exception of *E. faecalis*, which was grown in brain heart infusion
422 medium in standing flasks at 37°C, and *M. smegmatis*, which was also grown standing at 37°C
423 in LB broth with 0.05% Tween-80. Culture was diluted to a starting OD_{600} of 0.05. Bacteria were
424 incubated in the presence of an 8-point (2-fold) dilution series of each inhibitor ranging from 200
425 µM to 1.5 µM for 6 h, except for *M. smegmatis*, which was incubated for 72 h. Growth was

426 monitored by measuring optical density and normalized based on kanamycin (100% growth
427 inhibition) and DMSO (0% growth inhibition) controls, with the exception of *P. aeruginosa*, for
428 which 10 µg/mL tobramycin was used as the control for 100% growth inhibition. The
429 experiments were performed with three technical replicates per plate. EC_{50}s were calculated
430 based on a variable-slope four-parameter nonlinear least-squares regression model in the
431 GraphPad Prism software package (version 8).
432
433 **Kinetic Kill Curves**
434 Mtb was cultured in 7H9 medium to an OD_{600} of 0.5-1.0 and diluted to an OD_{600} of 0.1. In
435 triplicate, diluted samples were aliquoted into 96 well plates and inoculated with 20 µM
436 concentrations of each compound with DMSO as a negative control. Plates were placed in zip
437 lock bags with moistened paper towels and incubated at 37 ºC. Daily samples were taken and
438 serial diluted in 96 well plates using 1x PBS + 0.05% Tween-80 (v/v) and plated on 7H10
439 quadrant plates supplemented with OADC (10% v/v). Plates were incubated at 37ºC and
440 colonies were counted to calculate CFU/mL. Experiments were conducted in biological triplicate
441 and repeated at least twice.
442
443 **Isolation of Resistant Mutants**
444 Mtb was grown to an OD_{600} of 0.6-1.0 and samples were resuspended in fresh media for
445 a final cell count of 2 x 10^9 cells/ml. Cell pellets were resuspended in 0.5 ml of 7H9 medium and
446 plated on 7H10 OADC plates supplemented with 20 µM or 40 µM concentrations of HC2060,
447 HC2149, HC2169, and HC2184. Plates were incubated at 37 ºC until isolated colonies
448 appeared. Colonies were picked and inoculated into 5 ml of 7H9 medium in T25 standing flasks
449 and grown to an OD_{600} 0.5-1.0. Samples were taken and tested for resistance using dose
450 response curves described above along with WT grown to an OD_{600} of 0.6-1.0 and 3 µM RIF
451 and DMSO were used as controls. Samples were also serial diluted as described above and

452 plated for colony purified single colony isolates on X-plates containing 7H10 OADC. Single
453 colony isolates were picked and inoculated into 5 ml of 7H9 OADC in T25 flasks. Resistance
454 was re-confirmed using the same methods described above. Differences in EC_{50} values were
455 deemed significant based on the 95% confidence intervals.
456
457 **Whole Genome Sequencing and Analysis**
458 Whole genome sequencing was performed as previously described[44]. Briefly cultures of
459 single colony isolates were grown to an OD_{600} ~1.0 and pelleted. Genomic DNA was extracted
460 and sequenced by Illumina-based whole genome sequencing at 250 bp reads. Sequencing
461 results were analyzed using the GATK workflow for the identification of single nucleotide
462 variations[45].
463
464 **TMM and TDM accumulation assay**
465 The lipid assay was carried out as previously described(6). Briefly, 30 ml cultures of Mtb
466 was cultured to an OD_{600} of 0.6. Samples were diluted to an OD_{600} of 0.1 in 8 ml cultures in T25
467 flasks. Cultures were inoculated with 8 µCi of ^{14}C-acetate. Cultures were co-inoculated with 20
468 µM samples of MmpL3 inhibitors and then incubated for 24 hours before performing lipid
469 extraction as previously described[9]. Total extractable lipid ^{14}C-incorporation was determined by
470 scintillation counting, and 5,000 cpm of lipids were separated on TLC plates with a 24:1:0.5
471 Chloroform:Methanol:H_2O solvent system. TLCs plates were imaged using a Typhoon FLA 7000
472 and images were quantified using IQ image quantifying software. Experiments were conducted
473 in biological duplicate. Comparison to the DMSO controls was conducted using the T-test.
474
475 **Targeted whole cell phenotypic screening**
476 Each *mmpL3* mutant was cultured independently in 8 ml of 7H9 medium in T25 standing
477 flasks to an OD_{600} of 0.6 – 1.0. Mutant cultures were separately back diluted to an OD_{600} of 0.6

in 1.5 ml of 7H9 medium in 2 ml screw cap tubes. The contents of each tube were mixed into a single batch culture in a T75 culture flask. The mixed mutant culture was allowed to recover overnight (~8 hours) at 37°C. Samples of Mtb Erdman (WT, OD_{600} = 0.6) and the mixed mutant population were back diluted to an OD_{600} of 0.1 in 7H9 medium. WT and mutant pools were aliquoted, in technical duplicate, into separate clear bottom black walled 96 well plates. Samples of WT and mixed mutant cultures were inoculated with 20 μM of each of the 163 compounds from the small molecule library. Additional treatments included 0.5 μM samples of *para*-amino salicylic acid (PAS), SQ109, bedaquiline (BDQ), isoniazid (INH), clofazimine (CFZ), as well as DMSO and 0.3 μM RIF. Percent growth inhibition (%GI) of WT and mutant mix population were calculated for each treatment and hits were defined as 1) compounds with at least 15% GI in the WT background and 2) 1.5 fold decreased inhibition in the mutant pool relative to the WT background. The hit compounds were confirmed by conducting dose responses curves of screen hits as described above against WT and *mmpL3* mutant pools. Dose response curves were conducted in technical duplicate and differences between the WT and *mmpL3* mutant pool was deemed significant based on 95% confidence interval. Confirmed hits were reassessed with similar results.

Cross resistance studies were conducted by generating dose response curves for every combination of MmpL3 inhibitor and each *mmpL3* mutant, and WT Mtb strain, CDC1551 or Erdman depending on the background of the *mmpL3* strain (for a total of 338 dose response curves). Cross resistance dose responses were conducted singly, unless the dose response identified increased sensitivity in the *mmpL3* mutant background, in which case the responses were re-examined using dose responses carried out in biological duplicate. The dose responses were then used to calculate the area under the curve (AUC) using Prism 8 software using the default setting. AUCs were compare to the respective WT strains by dividing the AUC of the *mmpL3* strain by the respective WT parent strain. AUC fractions were then standardized by treatment by Z-scoring [19]. Z-score standardized data was then clustered in MatLab by

hierarchical agglomerative clustering using the *clustergram* function with default settings (Euclidean distance model, Average linkage clustering). Hierarchical agglomerative clustering using bootstrapped data was conducted in R using *pvclust* (nboot = 1000) using the Euclidean distance model and average linkage clustering [46].

Membrane Potential Assays

The $DiOC_2$ membrane potential assay was carried out as previously described [1, 9]. Briefly, Mtb Erdman cells were labeled with 30 µM DiOC2 (Thermo Scientific) in 1 ml of 1X phosphate-buffered saline (PBS) (pH 7.4), supplemented with 50 mM KCl, and incubated at 37°C for 15 min. Cells were washed twice and suspended in 1X PBS at a final concentration of an OD_{600} of 0.2, and 200 µL of labeled cells were aliquoted to 96-well plates and treated with each of the MmpL3 inhibitors at 80 µM, 20 µM, or 5 µM concentrations. Samples were also treated with DMSO (negative control) or 25 µM CCCP (Sigma-Aldrich) (positive control). Each treatment included three technical replicates per plate. The kinetics of fluorescence (excitation, 485 nm; emission, 610 nm/515 nm) was measured every 2 min for 60 min. The red/green (610 nm/515 nm) fluorescence intensity ratio was calculated and used to quantify membrane potential. The experiment was repeated at least twice with similar results. The error bars represent the standard deviation of the geometric mean.

Bactericidal Activity *in vitro* and in macrophages

An Mtb CDC1551 strain with a chromosomally encoded firefly luciferase [47] was grown to an OD_{600} of 0.6 – 1.0 in rich medium. For *in vitro* experiments cultures were diluted to an OD_{600} of 0.1 and aliquoted at 100µL in white walled 96 well plates and inoculated with compounds with each inhibitor, along with DMSO or RIF controls. The luciferase assay was carried out as previously described and plates were read on a PerkinElmer Enspire plate reader.

For studies in macrophages, primary bone marrow derived macrophages were harvested and infected as previously described [48]. Briefly, BMMΦ from C57Bl/6 mice were distributed into 96 well white plates and infected for 1 hour with a CDC1551 luciferase reporter strain[47]. Following 1 hour of infection, cells were treated with inhibitors ranging from 200 – 0.2 μM of MmpL3 inhibitors. 20 μM PAS, 3 μM RIF, and DMSO were used as controls. Samples were incubated in the 96 wells plates at 37ºC + 5% CO_2 for 6 days before carrying monitoring bacterial survival by measuring luciferase activity. Experiments were conducted in biological triplicate and repeated at least once with similar results.

Protein Modeling.

The 3D structure for MmpL3 was generated using the I-TASSER server[49]. The MmpL3 protein sequence of H37Rv from Mycobrowser (Rv0206c) [50] was aligned to the MmpL3 crystal structure of Msm (PDB: 6AJF) with a resulting C-score of 0.17 (TM-score 0.74 ± 0.11, RMSD 8.4 ± 4.5Å). The resulting structure was modified to remove the C-terminal tail (732/944AA) in PyMol 2.2.3 [51].

DiaMOND:

DiaMOND analysis was carried as described by Cokol *et al.,* with modifications as described (12). Briefly concentration ranges were linearized using the equation

$$\Delta D = \frac{M - m}{N - 1}$$

$$\Delta D = D_N - D_{N-1}$$

Where ΔD is the difference between concentrations of each dose, M is the lowest concentration to inhibit Mtb growth 100%, and m is the highest concentration estimated to confer 0% growth inhibition based on the EC_{50} dose response curves. N is the number of doses to be used in DiaMOND. Mtb was then treated with each concentration range for each compound by itself

554 (Null treatment) at a [X_N] or in combination with another inhibitor at a [½X_N]. Dose responses
555 were used to generate a dose response curve for each treatment which was used to interpolate
556 the IC_{50} which was set for the observed, "*o*" to calculate the FIC_2 ($FIC_2 = \frac{o}{e}$) as previously
557 described[37]. Dose responses were conducted in biological duplicate and reported FIC_2 values
558 are representative of the geometric mean of two reps.
559
560 **Eukaryotic Cytotoxicity**
561 Primary BMMΦ were isolated and distributed into white wall 96 well plates as described
562 above. Cells were treated with inhibitors ranging in concentration from 200 – 0.26 μM. Cells
563 were incubated at 37C for 3 or 6 days with 5% CO_2. Cytotoxicity was tested using the Cell Titer
564 Glow assay kit using the methods from the provider. For a negative control cells were treated
565 with 4% of TritonX-100 and DMSO as a positive control [28].
566
567 **Kinetic solubility and microsomal stability assay.**
568 The kinetic solubility assay was conducted as described by Bevan *et al.*[52] Briefly, the assay was
569 performed with 7-point (2-fold) dilutions from 200 μM - 3.125 μM for the compounds.
570 Mebendazole, benxarotene and aspirin were also included as controls. The drug dilutions were
571 added to PBS, pH 7.4, with the final DMSO concentration of 1%, and incubated at 37 °C for 2 h.
572 The absorbance at 620 nm was measured for each drug dilution to estimate of the compound
573 solubility. Three replicates were examined for each dilution. Mouse microsomal stability was
574 conducted as described by Obach [53] and presented as % remaining following 30 minutes.
575 Values greater than 100% are likely due to changes in the solubility of the compounds over the
576 course of the assay and represent high stability in microsomes.
577

578 **Acknowledgements**

579 We thank Bree Aldridge for assistance in designing the DiaMOND studies. Christopher Colvin
580 and Benjamin Johnson provided technical assistance in the initial prioritization of compounds.
581 Additional technical assistance was provided by Bilal Alewei and Tom Dexheimer, in the MSU
582 medicinal chemistry and screening cores to conduct the solubility and microsomal stability
583 studies. Research reported in this study was supported by start-up funding from Michigan State
584 University and AgBioResearch, and grants from the NIH-NIAID (U54AI057153, R21 AI1170181
585 and R01AI116605), the Bill and Melinda Gates Foundation (OPP1059227), a strategic
586 partnership grant from the MSU Foundation (14-SPG-Full-2966), and the Jean P. Schultz
587 Endowed Biomedical Research Fund at the MSU College of Human Medicine.

588

589 **Author Contributions**

590 JW and RBA designed the experiments and wrote the manuscript; GC conducted prioritization
591 assays; JW, EH, KC conducted the Mtb and spectrum of activity experiments; CC and TD
592 designed and conducted the *M. abscessus* experiments; and, EE directed the solubility and
593 microsomal stability studies. All authors reviewed the manuscript.

594

595 **Disclosures.**

596 RBA is the founder and owner of Tarn Biosciences, Inc., a company that is working to develop
597 new TB drugs.

598

TABLE 1 Characterization of MmpL3 Inhibitors

Compound	WT EC_{50} (μM)	*mmpL3* Mutant Pool EC_{50} (μM)	Relative EC_{50}	MΦ EC_{50}	Δψ Disruption	Cytotoxicity (CC_{50}) (μM)	Solubility (μM)	Microsome Stability (% remain 30 min)
HC2032	2.2	>80	>36	0.8	Yes	>100	18	102
HC2060	16.9	>80	>5	4.1	No	>100	>300	44
HC2091	6.2	>80	>13	2.2	No	>100	>300	45
HC2099	1.7	38.9	23	<0.3	No	>100	178	71
HC2134	1.4	>80	>57	7.3	Yes	>100	116	N.D.
HC2138	4.0	>80	>20	<0.3	Yes	>100	66	122
HC2149	6.6	>80	>12	3.6	Yes	>100	131	138
HC2169	1.8	>80	>44	<0.3	No	>100	17	168
HC2178	3.8	>80	>24	2.0	Yes	>100	>200	4
HC2183	3.2	59.9	19	3.0	No	>100	>200	25
HC2184	7.6	>80	>11	0.7	Yes	>100	>300	30
C215	11.2	57.5	5	4.0	Yes	14.3	87	62
SQ109	2.4	6.9	2	<0.3	Yes	N.D.	N.D.	N.D.

N.D. – Not determined

Relative EC_{50} is fold difference between WT vs. *mmpL3* mutant pool.

599

600

TABLE 2 EC_{50} Values for Spectrum of Activity of MmpL3 Inhibitors*

	HC2032	HC2060	HC2091	HC2099	HC2134	HC2138	HC2149	HC2169	HC2178	HC2184	C215
Mtb – Erdman	3.0	14.8	7.0	5.3	2.1	2.3	11	2.4	3.7	8.9	16.2
Mtb – CDC1551	2.4	12.8	6.3	4.8	1.5	2.0	10.5	2.2	2.3	7.6	14.3
Mab	34.5[a]	13.6[a]	96.5[a]	81.8[a]	81.9[a]	8.2[a]	-28[a]	-36[a]	13.5[a]	7.0[a]	2.3[a]
Msm	2.2	80	20[9]	0.9	1.8	N.D.	>200	13.2	4.5	85.7	>200
S. aureus (1)	>200	>200	>200[9]	>200	51.0	N.D.	>200	>200	>200	>200	15.1
S. aureus (2)	>200	>200	>200[9]	>200	51.8	N.D.	>200	>200	>200	>200	22.8
E. coli	>200	>200	>200[9]	>200	>200	N.D.	>200	>200	>200	>200	>200
P. vulgaris	>200	>200	>200[9]	>200	35.1	N.D.	>200	>200	>100	>200	>200
E. faecalis	>200	>200	>200[9]	>200	>200	N.D.	>200	>200	>200	>200	34
P. aeruginosa	>200	>200	>200[9]	>200	>200	N.D.	>200	>200	>200	>200	>200

*All values are EC_{50} except for *M. abscessus* data which are single concentration % inhibition data

a – Growth Inhibition (%) at 20μM

9 – Reference number of previously published data

Mab, *M. abscessus;* Msm, *M. smegmatis*

S. aureus (1) – *S. aureus* ATCC29213, *S. aureus* (2) – *S. aureus* ATCC25923

N.D. – not determined

601

602

603 **Figure Legends**

604 **Figure 1: Four compounds inhibit Mtb growth in a dose and time dependent manner. a)**
605 Structures of HC2060, HC2149, HC2169 and HC2184. **b)** Inhibition of Mtb growth in a dose
606 dependent manner. **c)** Killing of Mtb in a time dependent manner when treated at 20μM of the
607 inhibitors. Error bars indicate the standard deviation from the mean. Experiments were
608 conducted in biological triplicate.

609

610 **Figure 2: Modulation of TMM and TDM accumulation. a)** Whole cell ^{14}C-lipids from Mtb
611 treated with 20μM of HC2060, HC2149, HC2169 and HC2184 show increased levels of TMM
612 and decreased levels of TDM. **b and c)** Whole cell ^{14}C-lipid from Mtb treated with 20μM of the
613 six inhibitors identified by the targeted phenotypic screen show increased levels of TMM and
614 decreased levels of TDM. Experiments were conducted in biological duplicate. In both
615 experiments Mtb samples were treated with DMSO or 20μM SQ109. Error bars indicate the
616 standard deviation. p-value < 0.05 (*), <0.005 (**), <0.001 (***). ♦ indicates values that just
617 missed the cut off, HC2134 TMM p-value = 0.07. HC2060 and HC2149 missed significance
618 cutoffs, but this may be due to the high variability in reps as the relative there was a >2 fold in
619 difference for HC2060 and HC2149.

620

621 **Figure 3: A targeted whole cell phenotypic screen identifies six new MmpL3 inhibitors. a)**
622 Results of a direct head to head comparison of percent growth inhibition of WT Mtb or a pooled
623 *mmpL3* mutant population treated with 20μM of 163 compounds. Additional treatments included
624 0.5μM of BDQ, CFZ, INH, PAS, SQ109 or 0.03% H_2O_2. Examples of hit compounds with
625 reduced activity in the MmpL3 mutant pool are shown in red. **b)** Structures of the confirmed hits
626 from the screen, including six new compounds HC2032, HC2099, HC2134, HC2138, HC2178,

627 and HC2183. Previously described compounds include C215, HC2091 and SQ109 . Radio-
628 TLCs are shown in Supplemental Figure 3.
629
630 **Figure 4: Cross resistance profiling identifies clustering of compounds and mutations.**
631 Cluster analysis of cross-resistance profiling of twenty-four *mmpL3* strains treated with each of
632 the thirteen MmpL3 inhibitor normalized by Z-scoring by treatment. Compounds clustered into
633 two clades: Clade A and Clade B. Mutant strains, denoted by amino acid substitution, clustered
634 into two clades: Clade I and Clade II. Colors are based on Z-score normalization of treatment,
635 green indicates when treatments were less effective and red indicates when treatments were
636 more effective than the average (black). n.s. indicates a branch where the approximate
637 unbiased (AU) value was < 75. All other branches were significant based on bootstrap AU
638 values > 75.
639
640 **Figure 5: DiaMOND Analysis Identifies Additive, Synergistic and Antagonist Inhibitor**
641 **Interactions.** Hierarchical cluster analysis of DiaMOND-based pairwise inhibitor interactions of
642 all combinations of MmpL3 inhibitors and RIF identifies additive (FIC_2 0.82-1.18) antagonistic
643 (FIC_2 > 1.18) and synergistic (FIC_2 < 0.82) interactions.
644
645 **Figure 6: Mutation substitutions cluster according to cross resistance clades. a-d)** Front,
646 back, top, and bottom (respectively) views of an I-TASSER predicted structure of Mtb MmpL3
647 based on *M. smegmatis* MmpL3 structure (PDB: 6AJH). Substitutions conferred by mutations in
648 *mmpL3*. Substitutions are colored based on clade from cross resistance profiling, Clade I
649 substitutions (green), Clade II substitutions (red), or M649 (blue) which fell into both clades
650 depending on substitution. The model shows a truncated version (732/944aa) of the MmpL3
651 protein lacking the C-terminal tail.

References

1. Foss MH, *et al.* Diphenylether-Modified 1,2-Diamines with Improved Drug Properties for Development against Mycobacterium tuberculosis. *ACS infectious diseases* **2**, 500-508 (2016).

2. Grzegorzewicz AE, *et al.* Inhibition of mycolic acid transport across the Mycobacterium tuberculosis plasma membrane. *Nature chemical biology* **8**, 334-341 (2012).

3. La Rosa V, *et al.* MmpL3 is the cellular target of the antitubercular pyrrole derivative BM212. *Antimicrob Agents Chemother* **56**, 324-331 (2012).

4. Lun S, *et al.* Indoleamides are active against drug-resistant Mycobacterium tuberculosis. *Nat Commun* **4**, 2907 (2013).

5. Remuinan MJ, *et al.* Tetrahydropyrazolo[1,5-a]pyrimidine-3-carboxamide and N-benzyl-6',7'-dihydrospiro[piperidine-4,4'-thieno[3,2-c]pyran] analogues with bactericidal efficacy against Mycobacterium tuberculosis targeting MmpL3. *Plos One* **8**, e60933 (2013).

6. Shetty A, *et al.* Novel Acetamide Indirectly Targets Mycobacterial Transporter MmpL3 by Proton Motive Force Disruption. *Front Microbiol* **9**, (2018).

7. Stanley SA, *et al.* Identification of novel inhibitors of M. tuberculosis growth using whole cell based high-throughput screening. *ACS Chem Biol* **7**, 1377-1384 (2012).

8. Tahlan K, *et al.* SQ109 targets MmpL3, a membrane transporter of trehalose monomycolate involved in mycolic acid donation to the cell wall core of Mycobacterium tuberculosis. *Antimicrob Agents Chemother* **56**, 1797-1809 (2012).

9. Zheng HQ, Williams JT, Coulson GB, Haiderer ER, Abramovitch RB. HC2091 Kills Mycobacterium tuberculosis by Targeting the MmpL3 Mycolic Acid Transporter. *Antimicrob Agents Ch* **62**, (2018).

10. Dupont C, *et al.* A new piperidinol derivative targeting mycolic acid transport in Mycobacterium abscessus. *Mol Microbiol* **101**, 515-529 (2016).

11. Rao SPS, *et al.* Indolcarboxamide Is a Preclinical Candidate for Treating Multidrug-Resistant Tuberculosis. *Science Translational Medicine* **5**, (2013).

12. Zhang B, *et al.* Crystal Structures of Membrane Transporter MmpL3, an Anti-TB Drug Target. *Cell* **176**, 636-648 e613 (2019).

13. Chim N*, et al.* The Structure and Interactions of Periplasmic Domains of Crucial MmpL Membrane Proteins from Mycobacterium tuberculosis. *Chem Biol* **22**, 1098-1107 (2015).

14. Li W*, et al.* Therapeutic Potential of the Mycobacterium tuberculosis Mycolic Acid Transporter, MmpL3. *Antimicrob Agents Chemother* **60**, 5198-5207 (2016).

15. Xu ZJ, Meshcheryakov VA, Poce G, Chng SS. MmpL3 is the flippase for mycolic acids in mycobacteria. *P Natl Acad Sci USA* **114**, 7993-7998 (2017).

16. Yamaryo-Botte Y*, et al.* Acetylation of trehalose mycolates is required for efficient MmpL-mediated membrane transport in Corynebacterineae. *ACS Chem Biol* **10**, 734-746 (2015).

17. Belardinelli JM*, et al.* Structure-Function Profile of MmpL3, the Essential Mycolic Acid Transporter from Mycobacterium tuberculosis. *ACS infectious diseases* **2**, 702-713 (2016).

18. Varela C*, et al.* MmpL genes are associated with mycolic acid metabolism in mycobacteria and corynebacteria. *Chem Biol* **19**, 498-506 (2012).

19. Degiacomi G*, et al.* Essentiality of mmpL3 and impact of its silencing on Mycobacterium tuberculosis gene expression. *Sci Rep* **7**, 43495 (2017).

20. Li W*, et al.* MmpL3 as a Target for the Treatment of Drug-Resistant Nontuberculous Mycobacterial Infections. *Front Microbiol* **9**, 1547 (2018).

21. McNeil MB, Dennison D, Parish T. Mutations in MmpL3 alter membrane potential, hydrophobicity and antibiotic susceptibility in Mycobacterium smegmatis. *Microbiology* **163**, 1065-1070 (2017).

22. Lamichhane G, Tyagi S, Bishai WR. Designer arrays for defined mutant analysis to detect genes essential for survival of Mycobacterium tuberculosis in mouse lungs. *Infect Immun* **73**, 2533-2540 (2005).

23. Griffin JE, Gawronski JD, Dejesus MA, Ioerger TR, Akerley BJ, Sassetti CM. High-resolution phenotypic profiling defines genes essential for mycobacterial growth and cholesterol catabolism. *PLoS Pathog* **7**, e1002251 (2011).

24. Sacksteder KA, Protopopova M, Barry CE, 3rd, Andries K, Nacy CA. Discovery and development of SQ109: a new antitubercular drug with a novel mechanism of action. *Future Microbiol* **7**, 823-837 (2012).

25. Lee BS, Pethe K. Therapeutic potential of promiscuous targets in Mycobacterium tuberculosis. *Current Opinion in Pharmacology* **42**, 22-26 (2018).

26. Li W*, et al.* Novel insights into the mechanism of inhibition of MmpL3, a target of multiple pharmacophores in Mycobacterium tuberculosis. *Antimicrob Agents Chemother* **58**, 6413-6423 (2014).

27. Poce G, Consalvi S, Biava M. MmpL3 Inhibitors: Diverse Chemical Scaffolds Inhibit the Same Target. *Mini Rev Med Chem* **16**, 1274-1283 (2016).

28. Zheng H*, et al.* Inhibitors of Mycobacterium tuberculosis DosRST signaling and persistence. *Nature chemical biology* **13**, 218-225 (2017).

29. Johnson BK, Colvin CJ, Needle DB, Mba Medie F, Champion PA, Abramovitch RB. The Carbonic Anhydrase Inhibitor Ethoxzolamide Inhibits the Mycobacterium tuberculosis PhoPR Regulon and Esx-1 Secretion and Attenuates Virulence. *Antimicrob Agents Chemother* **59**, 4436-4445 (2015).

30. Coulson GB*, et al.* Targeting Mycobacterium tuberculosis Sensitivity to Thiol Stress at Acidic pH Kills the Bacterium and Potentiates Antibiotics. *Cell chemical biology* **24**, 993-1004 e1004 (2017).

31. Ioerger TR*, et al.* Identification of new drug targets and resistance mechanisms in Mycobacterium tuberculosis. *PLoS One* **8**, e75245 (2013).

32. Aggarwal D, Gupta A, Janmeja AK, Bhardwaj M. Evaluation of tuberculosis-associated chronic obstructive pulmonary disease at a tertiary care hospital: A case-control study. *Lung India* **34**, 415-419 (2017).

33. Garcia-Garcia V, Oldfield E, Benaim G. Inhibition of Leishmania mexicana Growth by the Tuberculosis Drug SQ109. *Antimicrob Agents Chemother* **60**, 6386-6389 (2016).

34. Biava M, Porretta GC, Manetti F. New derivatives of BM212: A class of antimycobacterial compounds based on the pyrrole ring as a scaffold. *Mini-Rev Med Chem* **7**, 65-78 (2007).

35. Ballell L*, et al.* Fueling open-source drug discovery: 177 small-molecule leads against tuberculosis. *ChemMedChem* **8**, 313-321 (2013).

36. Colan SD. The Why and How of Z Scores. *Journal of the American Society of Echocardiography* **26**, 38-40 (2013).

37. Cokol M, Kuru N, Bicak E, Larkins-Ford J, Aldridge BB. Efficient measurement and factorization of high-order drug interactions in Mycobacterium tuberculosis. *Sci Adv* **3**, e1701881 (2017).

38. Li W, Sanchez-Hidalgo A, Jones V, de Moura VC, North EJ, Jackson M. Synergistic Interactions of MmpL3 Inhibitors with Antitubercular Compounds In Vitro. *Antimicrob Agents Chemother* **61**, (2017).

39. Chen P, Gearhart J, Protopopova M, Einck L, Nacy CA. Synergistic interactions of SQ109, a new ethylene diamine, with front-line antitubercular drugs in vitro. *J Antimicrob Chemother* **58**, 332-337 (2006).

40. Su CC, Klenotic P, Bolla JR, Purdy G, Robinson C, Yu E. MmpL3 is a lipid transporter that binds trehalose monomycolate and phosphatidylethanolamine. *bioRxiv* **doi.org/10.1101/531160**, (2019).

41. Zhang B*, et al.* Crystal Structures of Membrane Transporter MmpL3, an Anti-TB Drug Target. *Cell* **176**, 636-+ (2019).

42. Bollenbach T. Antimicrobial interactions: mechanisms and implications for drug discovery and resistance evolution. *Curr Opin Microbiol* **27**, 1-9 (2015).

43. Singh N, Yeh PJ. Suppressive drug combinations and their potential to combat antibiotic resistance. *J Antibiot* **70**, 1033-1042 (2017).

44. Baker JJ, Abramovitch RB. Genetic and metabolic regulation of Mycobacterium tuberculosis acid growth arrest. *Sci Rep* **8**, 4168 (2018).

45. McKenna A*, et al.* The Genome Analysis Toolkit: a MapReduce framework for analyzing next-generation DNA sequencing data. *Genome Res* **20**, 1297-1303 (2010).

46. Suzuki R, Shimodaira H. Pvclust: an R package for assessing the uncertainty in hierarchical clustering. *Bioinformatics* **22**, 1540-1542 (2006).

47. Andreu N*, et al.* Optimisation of bioluminescent reporters for use with mycobacteria. *PLoS One* **5**, e10777 (2010).

48. Johnson BK, Abramovitch RB. Macrophage Infection Models for Mycobacterium tuberculosis. *Methods Mol Biol* **1285**, 329-341 (2015).

49. Yang J, Zhang Y. I-TASSER server: new development for protein structure and function predictions. *Nucleic Acids Res* **43**, W174-181 (2015).

50. Kapopoulou A, Lew JM, Cole ST. The MycoBrowser portal: a comprehensive and manually annotated resource for mycobacterial genomes. *Tuberculosis (Edinb)* **91**, 8-13 (2011).

51. Schrodinger LLC. The PyMOL Molecular Graphics System, Version 2.2. (ed^(eds) (2015).

52. Bevan CD, Lloyd RS. A high-throughput screening method for the determination of aqueous drug solubility using laser nephelometry in microtiter plates. *Analytical chemistry* **72**, 1781-1787 (2000).

53. Obach RS. Prediction of human clearance of twenty-nine drugs from hepatic microsomal intrinsic clearance data: An examination of in vitro half-life approach and nonspecific binding to microsomes. *Drug Metab Dispos* **27**, 1350-1359 (1999).

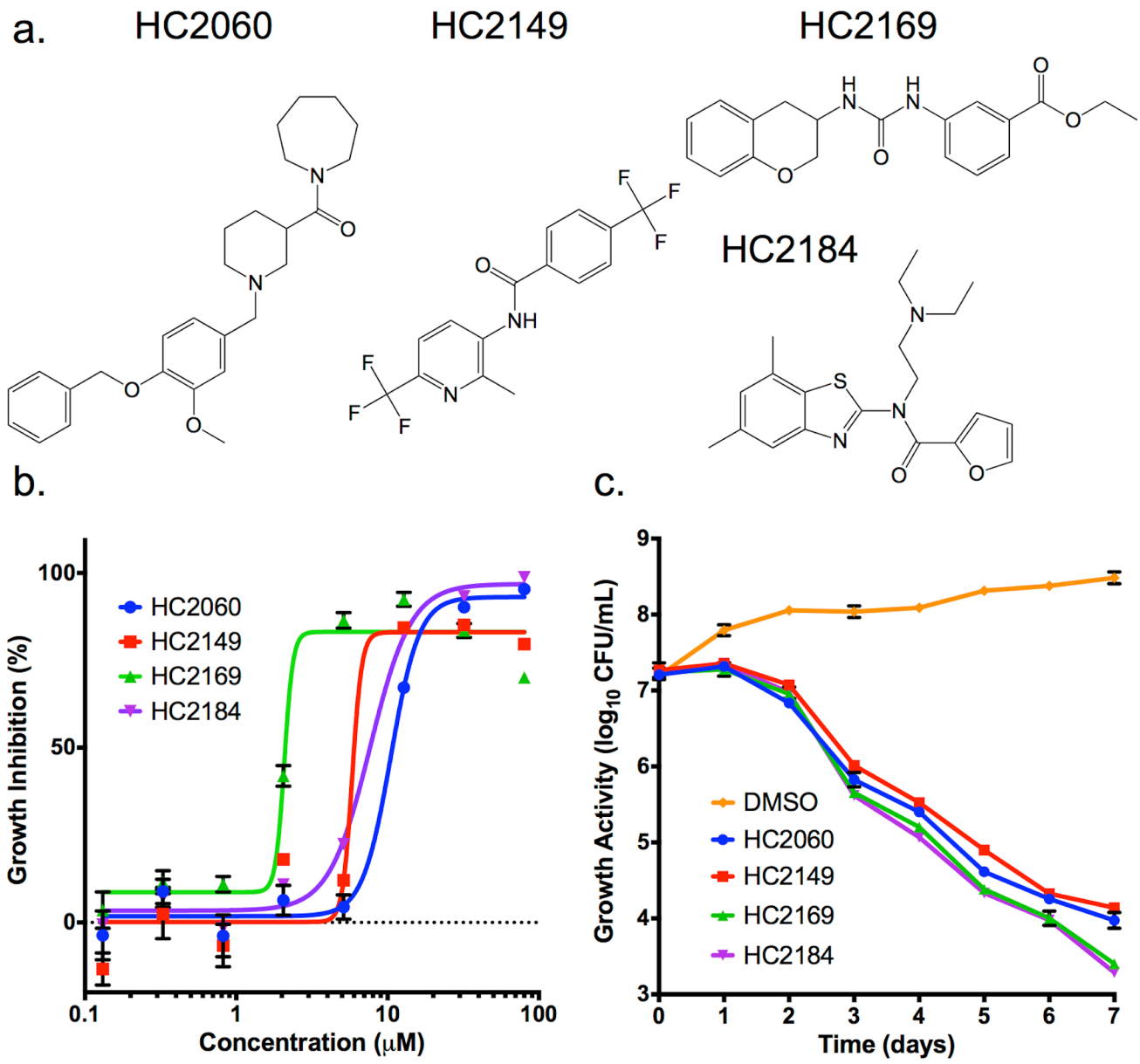

Figure 1

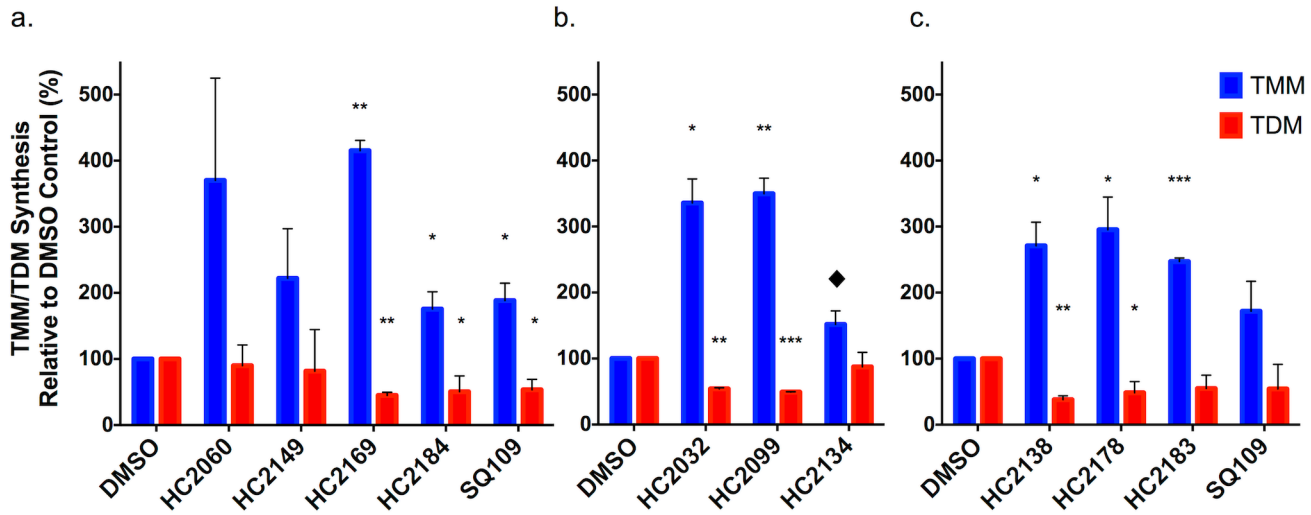

Figure 2

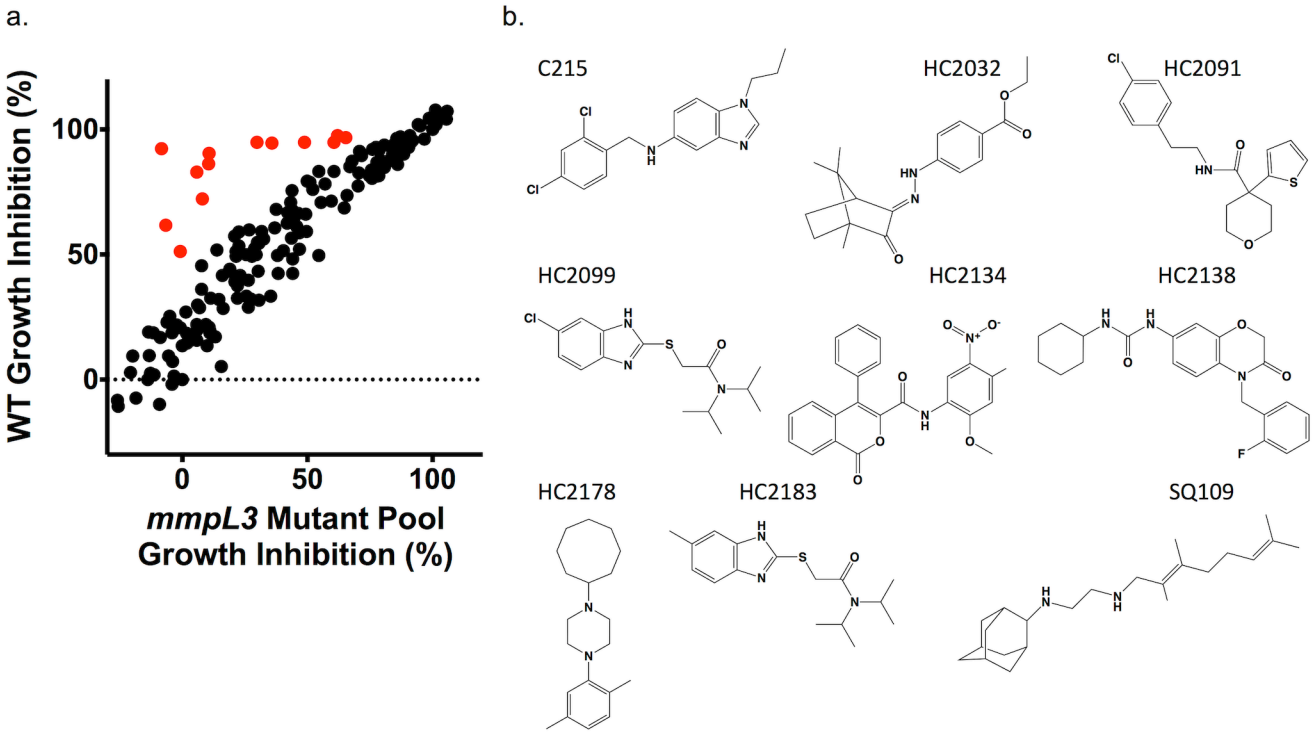

Figure 3

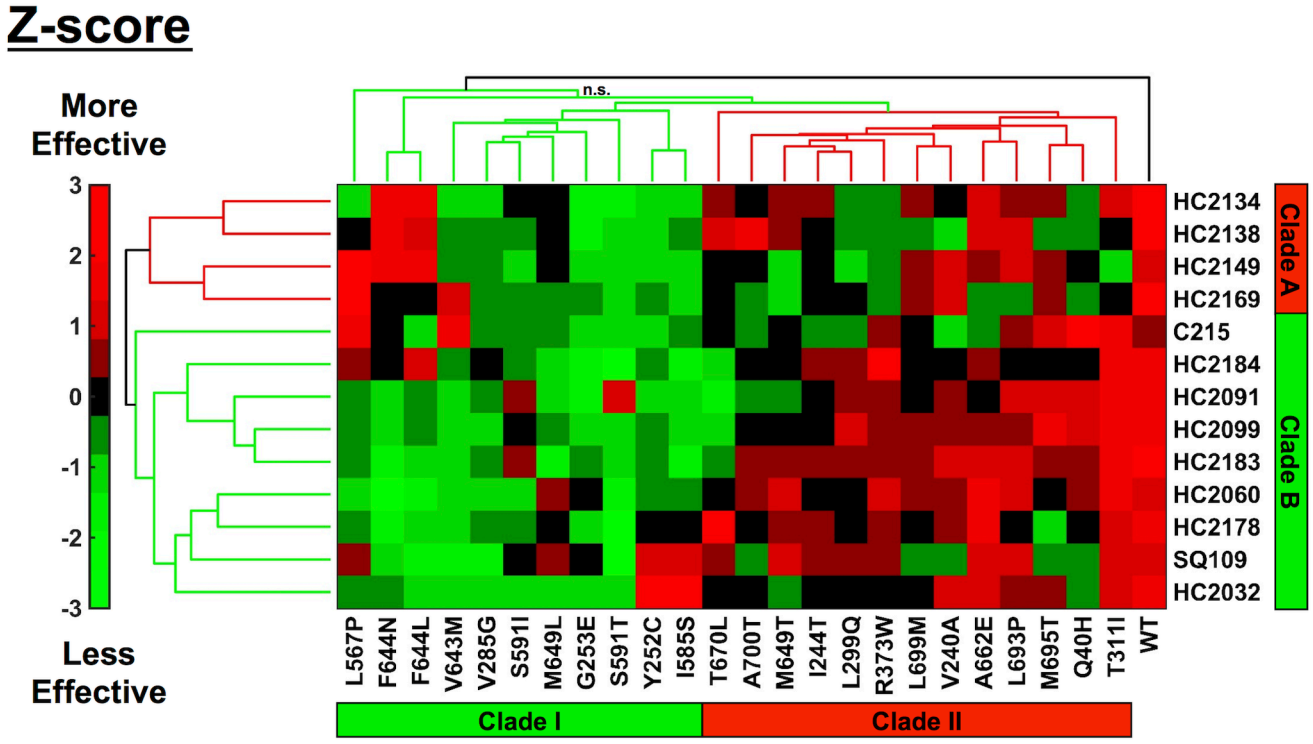

Figure 4

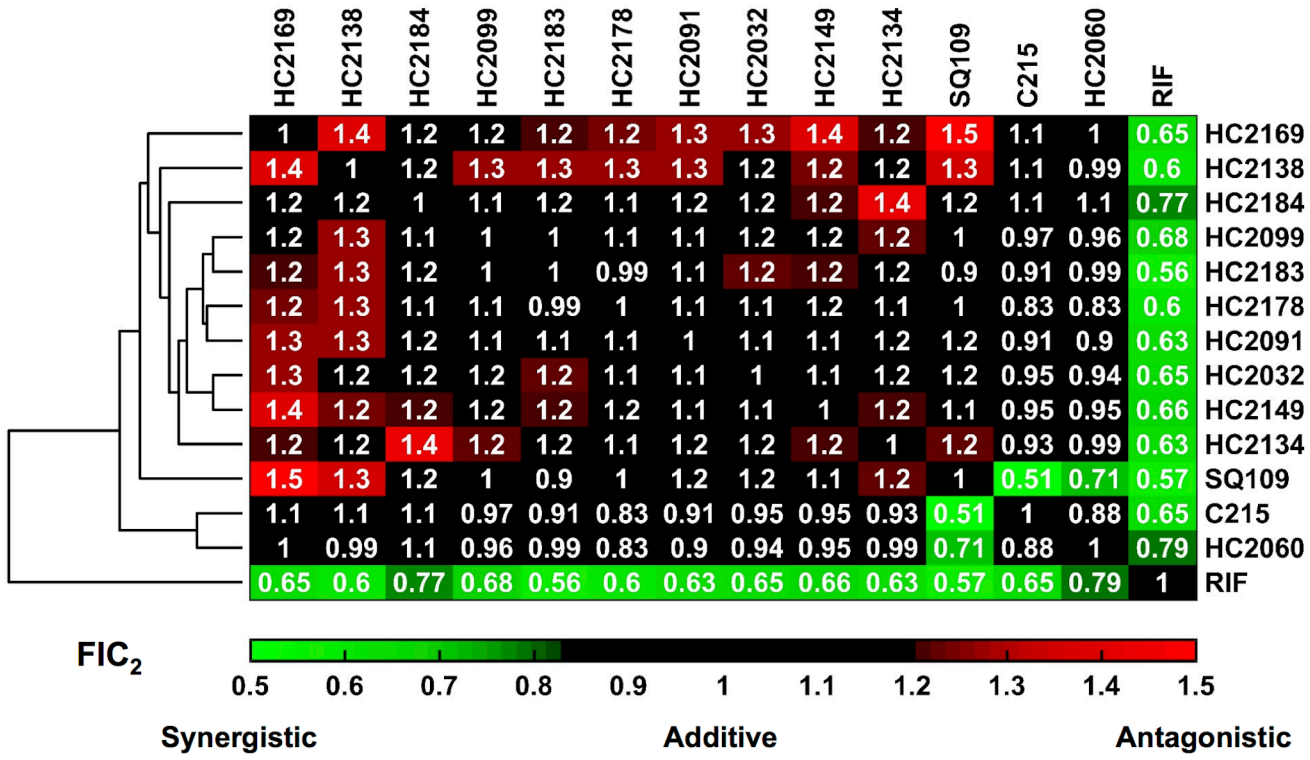

Figure 5

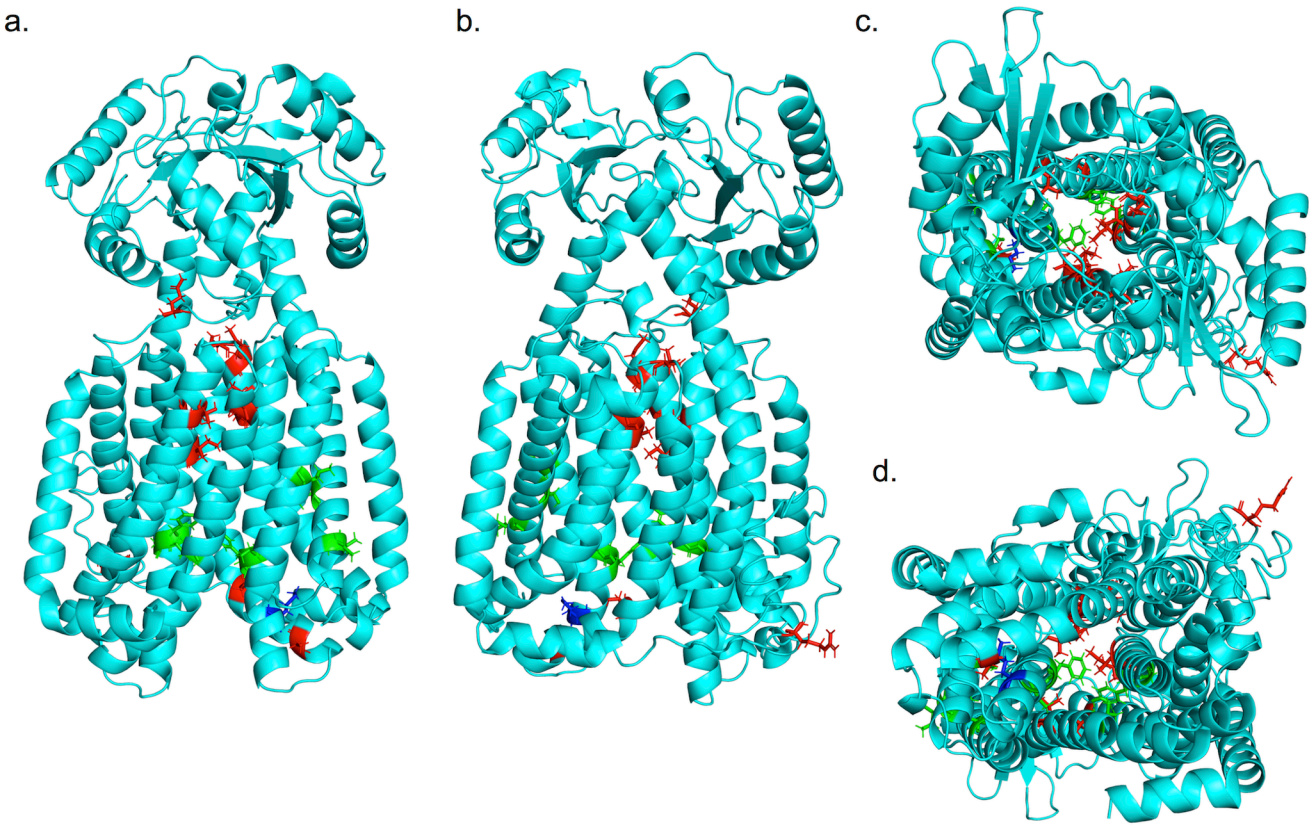

Figure 6

Supplemental Methods for *M. abscessus* spectrum of activity assays

Bacterial strains and culture media. For screens and hit confirmation, *Mycobacterium abscessus* Bamboo was used. *M. abscessus* Bamboo was isolated from the sputum of a patient with amyotrophic lateral sclerosis and bronchiectasis and was provided by Wei Chang Huang, Taichung Veterans General Hospital, Taichung, Taiwan. *M. abscessus* Bamboo whole genome sequencing showed that the strains belongs to *M. abscessus* subsp. *abscessus* and harbors an inactive clarithromycin-sensitive *erm* C28 sequevar (GenBank accession no. MVDX00000000). *M. abscessus* Bamboo cultures were grown in standard mycobacterium medium, Middlebrook 7H9 broth (BD Difco) supplemented with 0.5% albumin, 0.2% glucose, 0.085% sodium chloride, 0.0003% catalase, 0.2% glycerol, and 0.05% Tween 80. Solid cultures were grown on Middlebrook 7H10 agar (BD Difco) supplemented with 0.5% albumin, 0.2% glucose, 0.085% sodium chloride, 0.5% glycerol, 0.0003% catalase, and 0.006% oleic acid.

Single-point growth inhibition screening assay. The compound library was screened in microtiter plates as previously described with minor modifications. Briefly, the screen was carried out in 96-well flat-bottom Corning Costar plates at a single-point concentration of 20 μM with a starting inoculum of an optical density at 600 nm (OD_{600}) of 0.05 (10^7 CFU/ml) in a final volume of 200 μl. The culture for the starting inoculum was diluted from a preculture at mid-log phase (OD_{600}, 0.4 to 0.6). The plates were sealed using a Breathe-Easy sealing membrane (Sigma-Aldrich), put in an airtight container with moist tissue, and incubated for 3 days at 37°C on an orbital shaker at 110 rpm. Each plate had a medium-only control and a drug-free control, as well as positive control, clarithromycin at 20 μM. After 3 days of incubation, the cultures in the wells were manually resuspended before the OD_{600} was read in a TECAN Infinite Pro 200 plate reader. Compounds were scored according to their growth inhibition of the treated culture compared to the untreated culture (DMSO-treated). The experiment was conducted in duplicate, and the

results are shown as a scatter plot, with each data point representing the mean of data from the two replicates for each compound (Fig. 1).

Growth inhibition dose-response assay. MICs in dose-response assays were determined by the broth microdilution method as described previously (63), with some modifications. Briefly, 96-well plates were filled with 100 μl of 7H9 medium in each well. Two times the desired two-fold (10 points) serial dilutions of compounds were prepared with TECAN D300e Digital Dispenser. An appropriate dilution of a mid-log-phase culture to an OD_{600} of 0.1 (final OD_{600} in all wells was 0.05) was carried out, and 100 μl of the bacterial culture was added to the wells. The plates were incubated at 37°C and 110 rpm on an orbital shaker for 3 days and then manually resuspended, and the OD_{600} was measured using the plate reader. We report MIC_{50}s and MIC_{90}s which are the concentrations that inhibit 50% and 90% of growth respectively compared to the untreated control. The MIC_{90}s correspond to the standard “no visible growth” MICs. All experiments were carried with biological replicates as well as technical replicates.

Supplemental Figure Legends

Figure S1: Prioritization funnel of growth inhibitors from a high throughput screen. A high throughput screen of 273,000 compounds identified 1087 compounds that inhibit Mtb growth independent of the targeted two component regulators at 10 μM. These compounds were further tested as being able to inhibit Mtb growth (confirmed hits), have low eukaryotic cytotoxicity (<10%), able to inhibit intracellular Mtb growth (>25%) resulting in 216 compounds that meet the minimum requirements. Of the 216 compounds 163 commercially available compounds were purchased as fresh powders.

Figure S2: Resistant Mutants to Four Novel Inhibitors Map to mmpL3. a-d) Dose response curves of resistance mutant to four novel Mtb growth inhibitors. Curves are based on 2.5 dilutions of inhibitors ranging from 80 to 0.13μM. Experiments were conducted in triplicate and the error bars indicated the standard deviation of the mean. e) Transmembrane domain map shows diversity of substitutions conferred by mutations in mmpL3. Transmembrane domain map is based on Phyre2 analysis of H37Rv MmpL3 protein sequence. f) Venn Diagram identifies novel MmpL3 substitutions identified in this study. A total of 21 MmpL3 amino acid substitutions were identified in this study, including 14 novel substitutions and 7 previously identified substitutions (see TABLE S1 for list of substations).

Figure S3. TLCs show TMM/TDM Modulation. a-c) Mtb cells were grown in the presence of 8μCi of 14C-acetate for twenty four hours and treated with 20μM of **a)** the four prioritized inhibitors (HC2060, HC2149, HC2169 or HC2184) or **b and c)** the six inhibitors identified from the targeted mutant phenotypic screen (HC2032, HC2099, HC2134, HC2138, HC2178, HC2183). Lipids were isolated from whole cell extracts and analyzed by TLC. In each experiment samples of cells were also treated with either 20μM of SQ109 or DMSO.

Figure S4. Illustrated Outline of Targeted Mutant Phenotypic Screen. a) Growth inhibition of a pooled culture of twenty four unique *mmpL3* mutant strains of Mtb (multicolored suns) is directly compared with WT Mtb strains. Samples of either pooled *mmpL3* mutant strains or WT Mtb are aliquoted into separate 96 well plates and treated with 163 prioritized Mtb growth inhibitors, as well as BDQ, CFZ, INH, PAS, SQ109 and H_2O_2. Growth inhibition (%) is calculated as the growth inhibition relative to the DMSO and RIF controls. **b)** Beehive plot of relative fold decrease in activity of compounds in the mixed *mmpL3* mutant background compared to WT treated cells. Dotted line indicates a 1.5 fold resistance in the *mmpL3* mixed mutant background relative to the WT. Error bars (red) indicate the 95% confidence interval of the geometric mean.

Figure S5. 13 Dose response curves of thirteen proposed MmpL3 inhibitors on pooled mmpL3 mutant strains. a-m) Dose response curves of thirteen Mtb growth inhibitors confirmed to have reduced activity in the pooled mmpL3 mutant background (red) compared to WT Mtb (blue). Samples were treated with a series of (2.5 fold dilutions) of each inhibitor ranging form 80μM to 0.13μM. Growth inhibition (%) is calculated as the growth inhibition relative to the DMSO and RIF controls. Experiments were conducted in triplicate and error bars indicate the standard deviation from the mean.

Figure S6. Impact of Non-MmpL3 inhibitors on pooled mmpL3 mutant strains. Dose response curves of thirteen Mtb growth inhibitors confirmed to have reduced activity in the pooled mmpL3 mutant background (red) compared to WT Mtb (blue). Samples were treated with a series of (2.5 fold dilutions) of each inhibitor ranging form 80μM to 0.13μM. Growth inhibition (%) is calculated as the growth inhibition relative to the DMSO and RIF controls. Samples were run in triplicate and error bars indicate the standard deviation from the mean.

Figure S7. Capacity of Inhibitors to Disrupt Membrane Potential. a-m) Mtb cells labeled with DiOC2 and treated with 80μM (blue circle), 20μM (red square) or 5μM (green triangle) of each of the thirteen MmpL3 inhibitors for one hour. As controls DMSO (negative, purple inverted triangles)

and CCCP (positive, orange diamonds) treatments were also included. Experiments were carried out using the $DiOC_2$ membrane potential assay kit. The experiment was repeated twice with similar results. Data points are the geometric mean of three technical repeats. Error bars indicate the geometric standard deviation of three technical replicates. The experiment was repeated with similar results.

Figure S8. Bactericidal activity of MmpL3 Inhibitors. Mtb CDC1551 luc reporter strains were treated with a series of dilutions (2.5 fold) from 80 to 0.13μM of each of the thirteen MmpL3 inhibitors for six days in vitro. Cells were then tested for luciferase expression using the Bright-Glo Luciferase assay kit. Growth inhibition (%) is the normalized luciferase activity relative to the DMSO – positive and RIF – negative controls. Experiments were conducted in triplicate and the error bars indicated the standard deviation of the mean.

Figure S9. Impact of MmpL3 Inhibitors on Intracellular Growth. Primary bone marrow macrophages were infected with Mtb CDC1551 luc reporter strains. Infected macrophages were treated with a series of dilutions (2.5 fold) from 200 to 0.3μM of each of the thirteen MmpL3 inhibitors for six days in vitro. Cells were then tested for luciferase expression using the Bright-Glo Luciferase assay kit. Growth inhibition (%) is the normalized luciferase activity relative to the DMSO – positive and RIF – negative controls. Experiments were conducted in triplicate and the error bars indicated the standard deviation of the mean.

Figure S10. Clade substitutions Differ in Proximity to Essential Residues. a-d) Front, back, top, and bottom (respectively) views of an I-TASSER predicted structure of Mtb MmpL3 based on MmpL3 structure of Msm (PDB: 6AJH). Substitutions conferred by mutations in *mmpL3*. Substitutions are colored based on clade from cross resistance profiling, Clade I substitutions (green), Clade II substitutions (red), or M649 (blue) which fell into both clades depending on substitution. Yellow spheres indicate the seven essential residues (D251, S288, G543, D640,

Y641, D710, and R715) for MmpL3 activity identified by Bellardinelli and colleagues[17]. The model shows a truncated version (732/944aa) of the MmpL3 protein lacking the C-terminal tail.

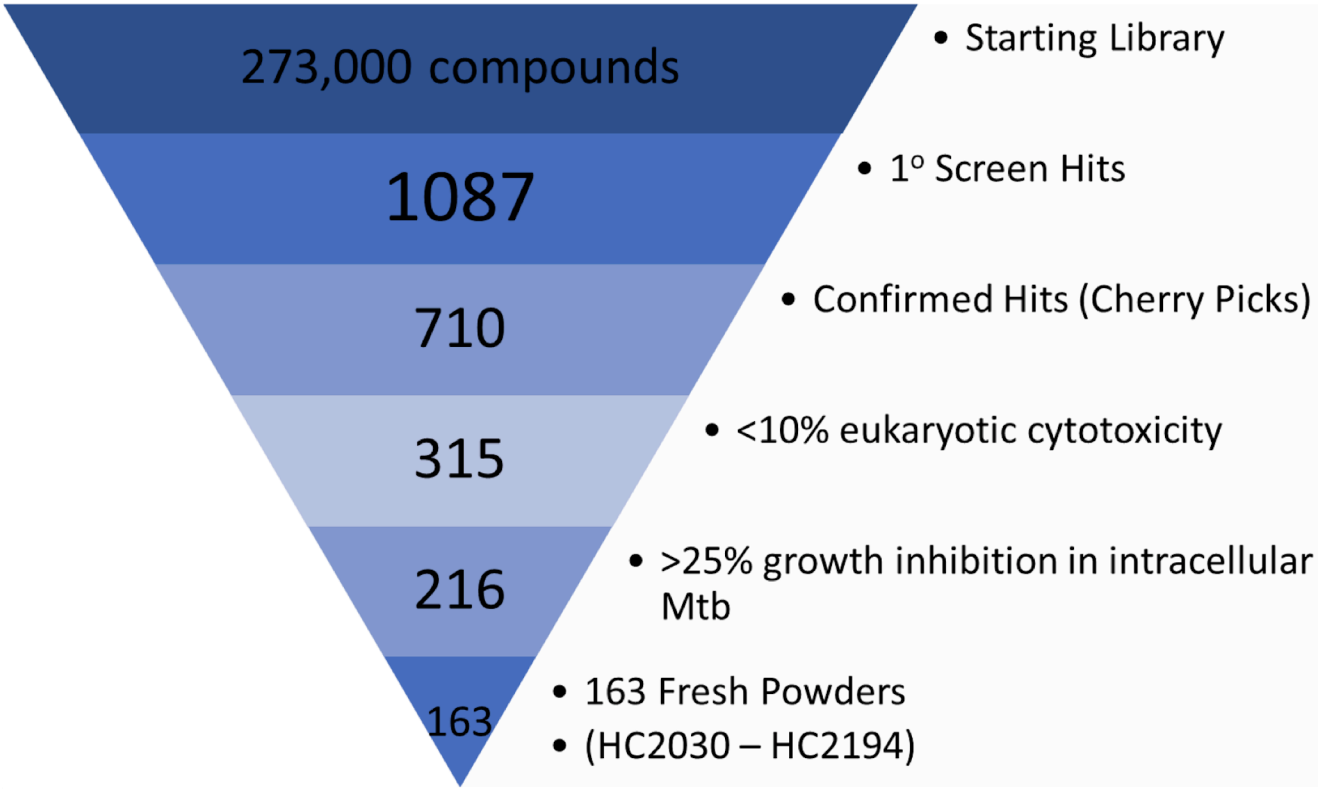

Figure S1

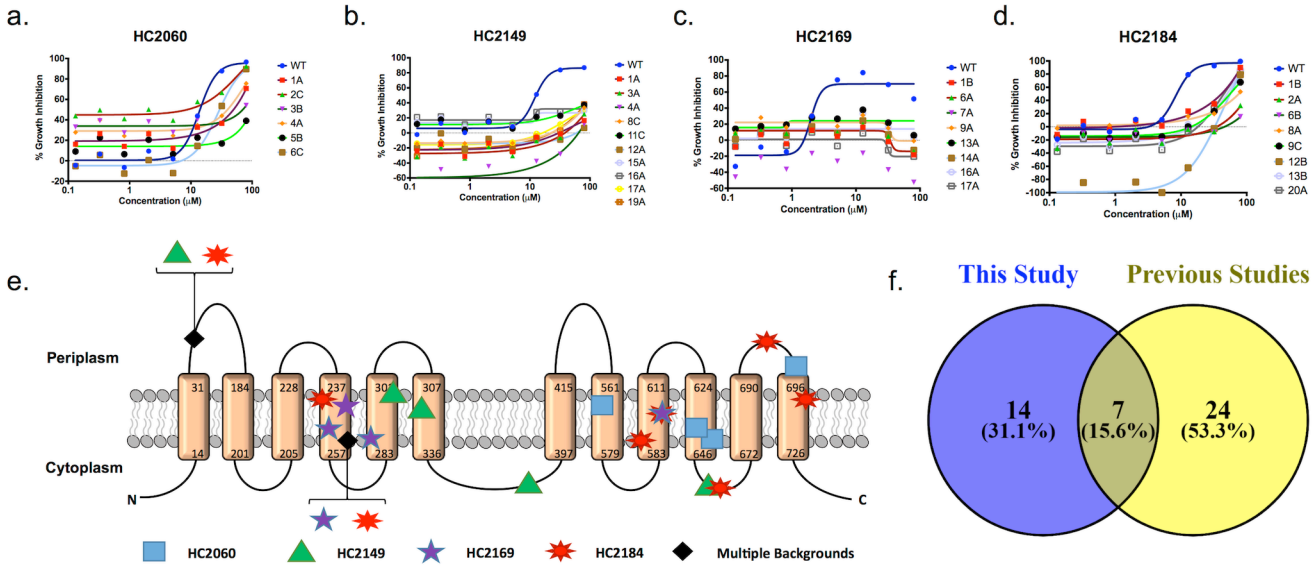

Figure S2

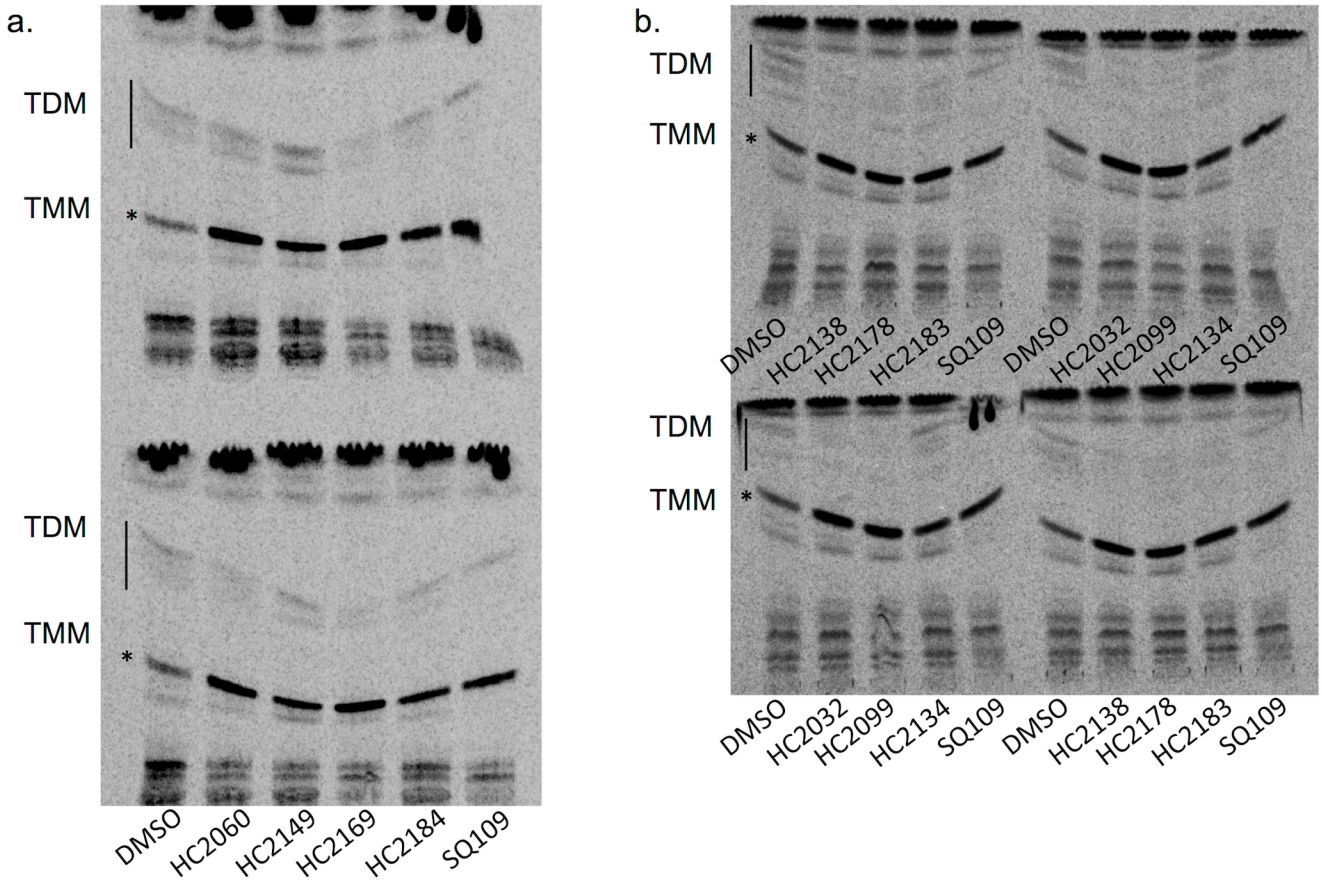

Figure S3

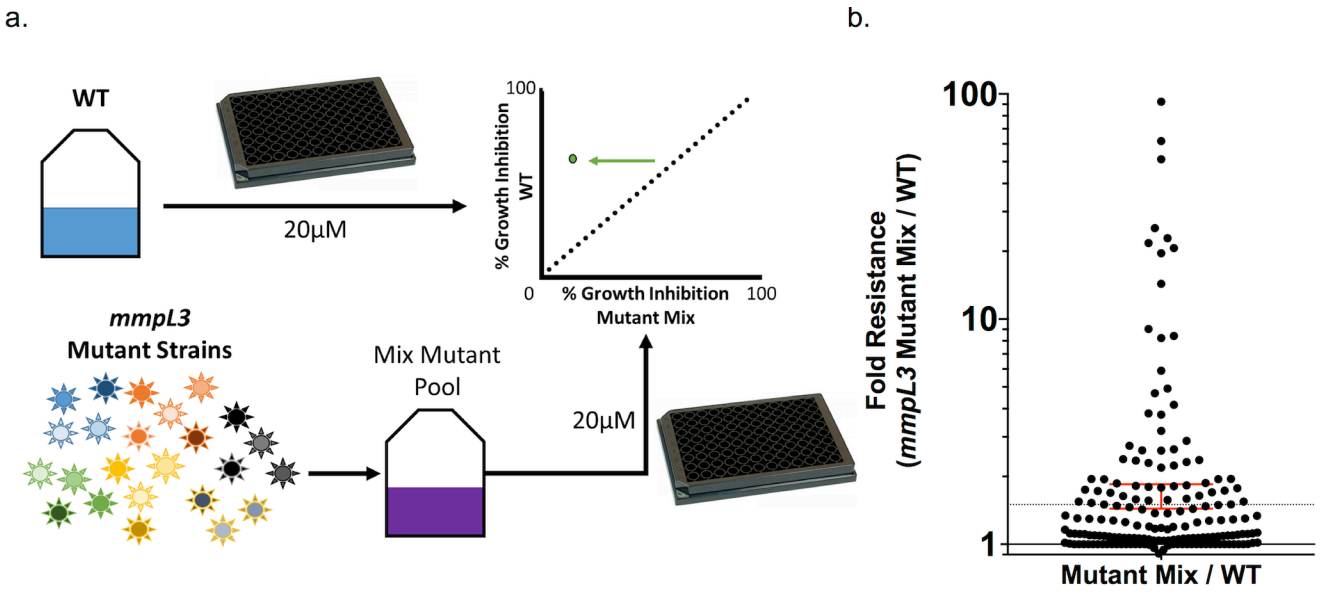

Figure S4

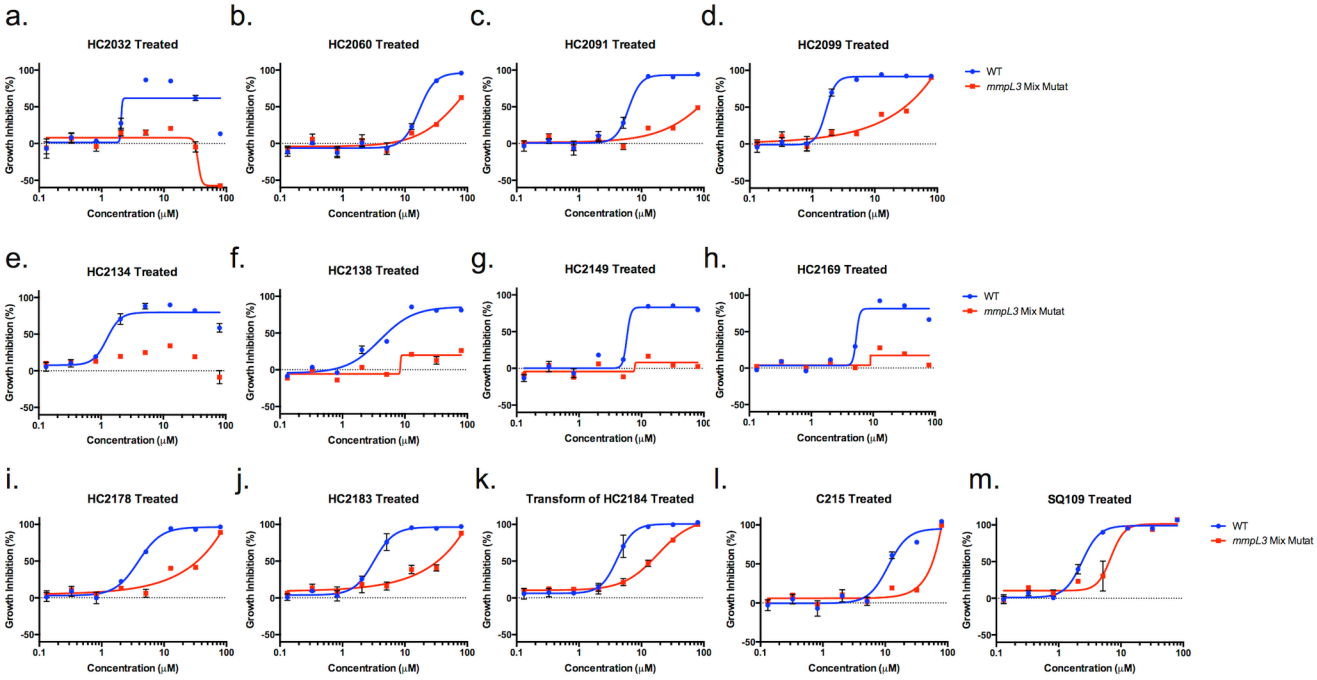

Figure S5

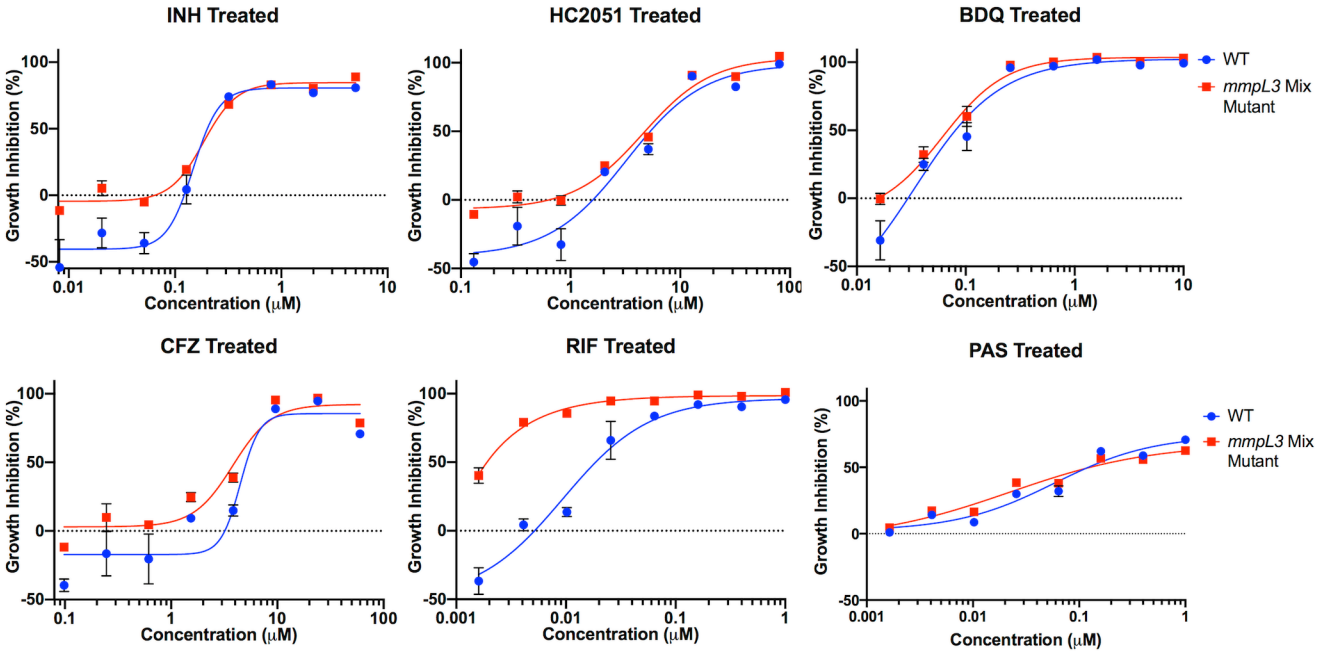

Figure S6

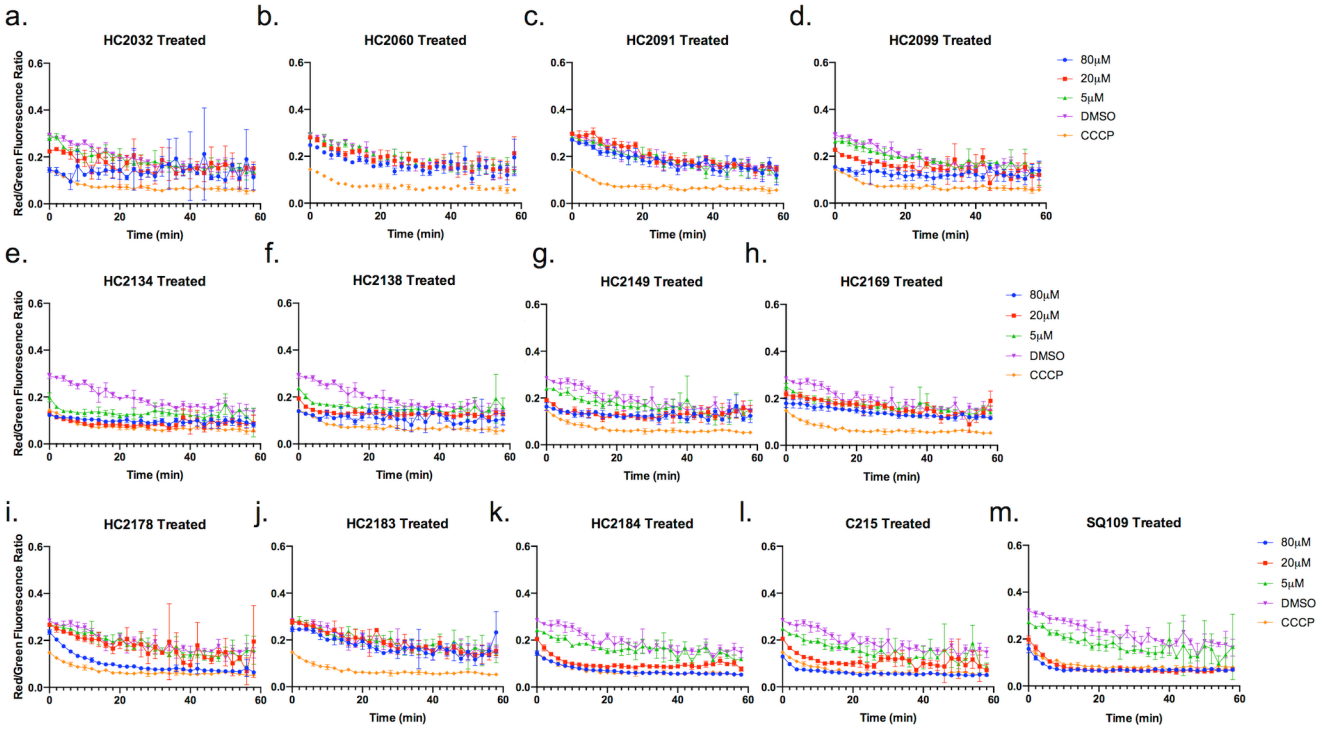

Figure S7

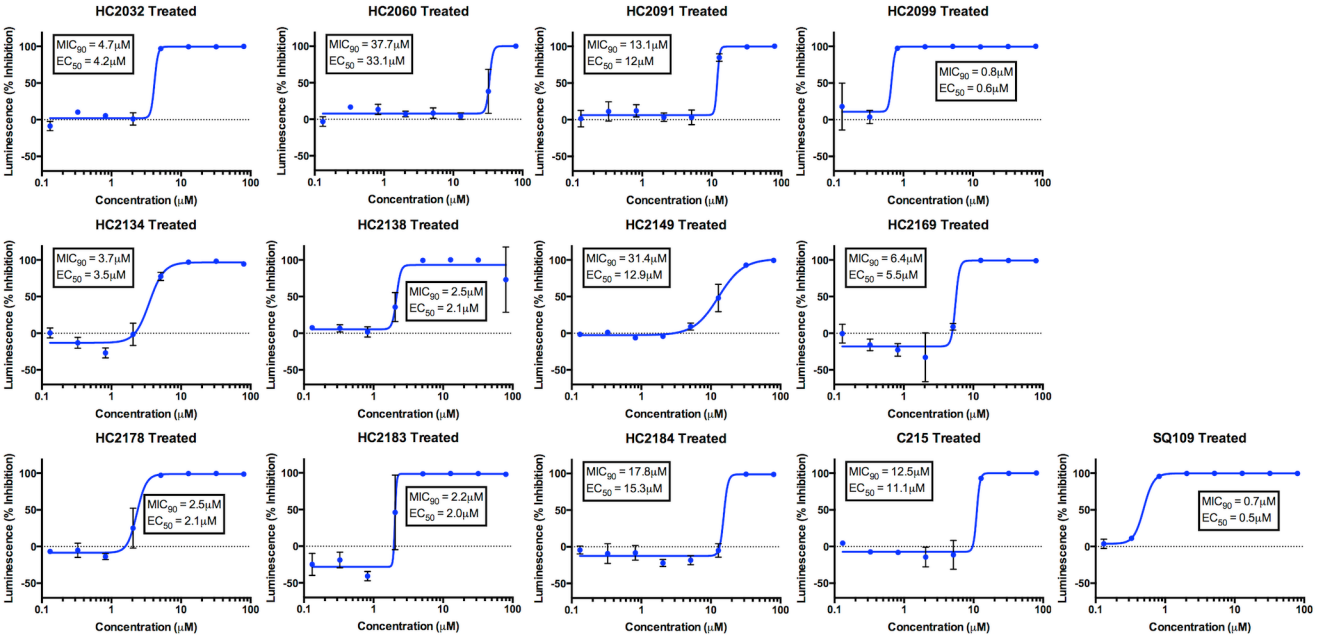

Figure S8

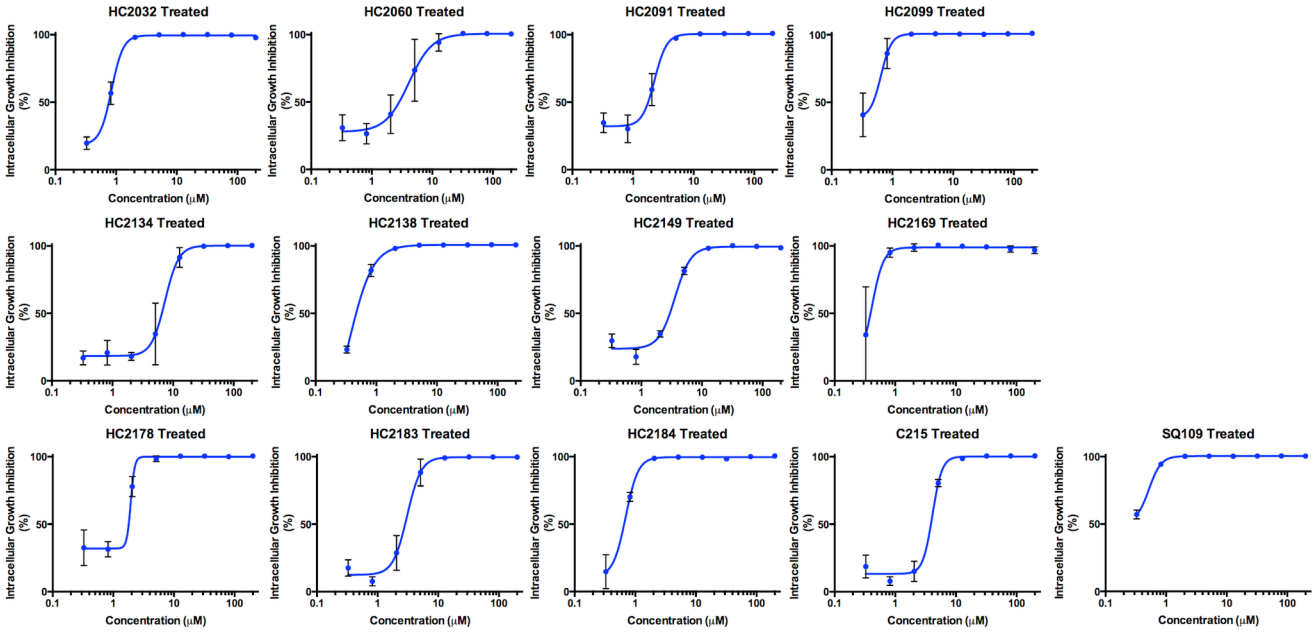

Figure S9

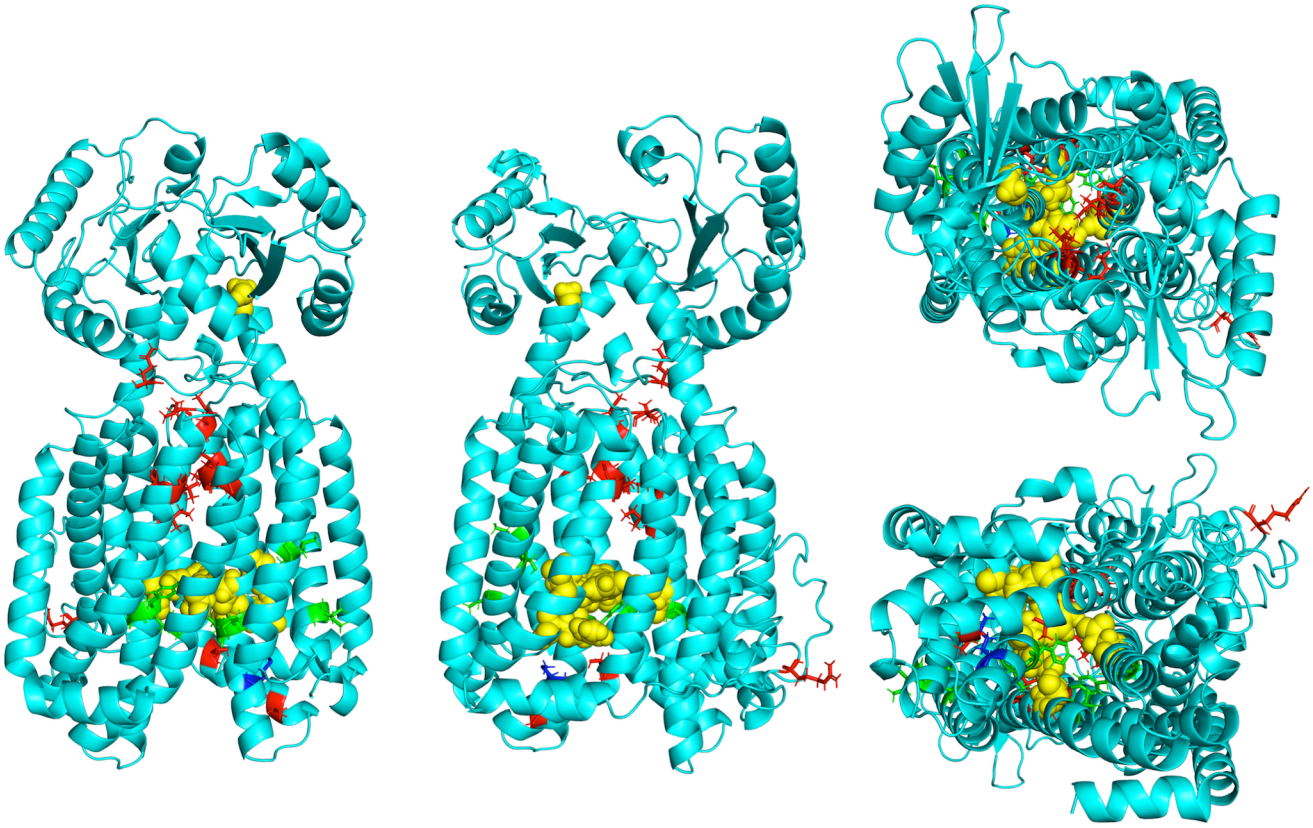

Figure S10

TABLE S1 Sequencing Results of Resistant Mutants

Compound	Strain	SNP Location (nt)	Quality Score	Gene	Nucleotide Change	AA Change
HC2060	1A / 2C	245506	5308 / 4597	*mmpL3*	GTG --> **A**TG	V643M
	3B	245501	4710	*mmpL3*	TTC --> TT**G**	F644L
	4A	245733	3840	*mmpL3*	CTG --> C**C**G	L567P
	5B	245501	4807	*mmpL3*	TTC --> TT**A**	F644N*
	6C	245349	4795	*mmpL3*	ATG --> A**C**G	M695T*
HC2149	1A	245487	5798	*mmpL3*	ATG --> A**C**G	M649T*
	3A / 4A / 8C / 17A / 19A	247313	5895 / 6057 / 5228 / 4998 / 5725	*mmpL3*	CAG --> CA**T**	Q40H*
	11C / 12A	246316	5127 / 6751	*mmpL3*	CGG --> **T**GG	R373W*
	15A	246501	3836	*mmpL3*	ACC --> A**T**C	T311I*
	16A	246537	3854	*mmpL3*	CTG --> C**A**G	L299Q*
HC2169	1B / 6A / 17A	245662	7164 / 6152 / 6805	*mmpL3*	TCG --> **A**CG	S591T*
	14A	246579	4739	*mmpL3*	GTG --> G**G**G	V285G*
	13A	246675	4585	*mmpL3*	GGG --> G**A**G	G253E
	7A / 9A	246678	6076 / 4312	*mmpL3*	TAC --> T**G**C	Y252C*
	16A	246702	5280	*mmpL3*	ATC --> A**C**C	I244T*
HC2184	1B	245355	5122	*mmpL3*	GAC --> G**G**C	L693P*
	2A	246675	6093	*mmpL3*	CCC --> C**T**C	G253E
	6B	245661	5719	*mmpL3*	TCG --> T**A**G	S591I
	8A	246678	5654	*mmpL3*	ATG --> A**C**G	I585S*
	9C	247313	5824	*mmpL3*	GTC --> GT**G**	Q40H*
	12B	245338	5281	*mmpL3*	GAC --> **T**AC	L699M
	13B	245448	5121	*mmpL3*	CGC --> C**T**C	A662E*
	20A	246714	3800	*mmpL3*	CAC--> C**G**C	V240A*

* - Novel substitutions not previously identified in Mtb

TABLE S2 Genetic background of Mtb strains used in Screen

Compound Background	Mtb Strain Background	Strain	SNP Location	Quality Score	Gene	Nucleotide Change	Amino Acid Substitution
HC2060	Erdman	1A	245506	5308	*mmpL3*	GTG --> **A**TG	V643M
	Erdman	3B	245501	4710	*mmpL3*	TTC --> TT**G**	F644L
	Erdman	4A	245733	3840	*mmpL3*	CTG --> C**C**G	L567P
	Erdman	5B	245501	4807	*mmpL3*	TTC --> TT**A**	F644N
	Erdman	6C	245349	4795	*mmpL3*	ATG --> A**C**G	M695T
HC2091	CDC 1551	3A	245488	3441	*mmpL3*	ATG --> **C**TG	M649L
	CDC 1551	5A	245424	2685	*mmpL3*	ACC --> A**A**C	T670L
	CDC 1551	23A	245335	2615	*mmpL3*	GCC --> **A**CC	A700T
HC2149	Erdman	1A	245487	5798	*mmpL3*	ATG --> A**C**G	M649T
	Erdman	3A	247313	5895	*mmpL3*	CAG --> CA**T**	Q40H
	Erdman	11C	246316	5127	*mmpL3*	CGG --> **T**GG	R373W
	Erdman	15A	246501	3836	*mmpL3*	ACC --> A**T**C	T311I
	Erdman	16A	246537	3854	*mmpL3*	CTG --> C**A**G	L299Q
HC2169	Erdman	1B	245662	7164	*mmpL3*	TCG --> **A**CG	S591T
	Erdman	14A	246579	4739	*mmpL3*	GTG --> G**G**G	V285G
	Erdman	13A	246675	4585	*mmpL3*	GGG --> G**A**G	G253E
	Erdman	7A	246678	6076	*mmpL3*	TAC --> T**G**C	Y252C
	Erdman	16A	246702	5280	*mmpL3*	ATC --> A**C**C	I244T
HC2184	Erdman	1B	245355	5122	*mmpL3*	GAC --> G**G**C	L693P
	Erdman	6B	245661	5719	*mmpL3*	TCG --> T**A**G	S591I
	Erdman	8A	246678	5654	*mmpL3*	ATG --> A**C**G	I585S
	Erdman	12B	245338	5281	*mmpL3*	GAC --> **T**AC	L699M
	Erdman	13B	245448	5121	*mmpL3*	CGC --> C**T**C	A662E
	Erdman	20A	246714	3800	*mmpL3*	CAC--> C**G**C	V240A

TABLE S3 – EC_{50} Values of Control Compounds

Treatment	WT EC_{50}	Mix Mutant EC_{50}	95% Confidence Interval
INH	0.15	0.18	n.s.
HC2051	3.2	4.5	n.s.
CFZ	4.4	3.8	n.s.
BDQ	0.03	0.06	n.s.
RIF	0.009	<0.009	N.D.
PAS	0.05	0.02	n.s.

n.s. – Not significant
N.D. – Not determined

Table S4 – AUC Values from Cross Resistance Profiling

	HC2032	HC2060	HC2091	HC2099	HC2134	HC2138	HC2149	HC2169	HC2178	HC2183	HC2184	C215	SQ109
Q40H[E]	42.98	68.03	84.3	101.8	63.23	37.49	44.07	42.17	92.35	96.53	63.86	131.7	143
V240A[E]	102.2	82.81	73.08	89.43	68.44	15.86	77.88	94.26	108.7	107.7	68.1	26.77	143.3
I244T[E]	110.9	69.62	60.8	67.29	86.09	65.59	58.91	52.76	97.73	96.78	73.2	33.41	132.8
T252C[E]	149.4	48.76	27.29	55.58	35.23	14.64	23.38	35.96	87.77	60.9	58.37	18.72	181.4
G253E[E]	18.23	60.32	18.2	44.63	11.15	7.195	10.61	29.13	54.42	57.9	32.29	15.03	146
V285G[E]	31.87	40.62	39.38	48.43	29.35	34.77	34.81	41.29	78.09	57.41	59.12	33.96	117.1
L299Q[E]	95.93	85.39	72.67	90.14	59.81	37.88	21.73	55.48	91.53	93.22	73.78	40.02	157.2
T311I[E]	94.83	84.38	101.8	115.7	106.2	68.61	23.31	54.41	114.1	123.6	96.01	127.8	167.8
R373W[E]	62.68	78.36	70.65	79.96	53.12	85.28	37.85	35.57	105.8	91.78	100.1	62.15	157.2
L567P[E]	43.81	40.82	40.23	52.93	35.96	69.17	120.2	157.9	80.5	61.52	69.83	137.5	157.3
I585S[E]	165.1	47.59	26.81	40.55	31.87	53.06	23.38	19.76	90.54	34.68	35.16	31.11	201.3
S591I[E]	28.78	21.79	76.97	38.94	18.47	18.89	12.86	22.95	35.47	55.81	28.15	11.45	110.7
S591T[E]	31.85	39.27	66.47	65.59	68.16	43.98	24.29	28.08	80.44	90.53	50.04	32.04	144.8
V643M[E]	33.28	40.88	28.28	41.06	36.34	48.63	38.99	98.7	56.54	46.87	54.33	88.44	117.9
F644L[E]	34.12	21.31	25.91	48.32	130.9	123.7	93.34	58.46	51.75	38.31	65.11	48.58	132.2
F644N[E]	25.76	27.24	38.88	53.13	123.5	101.5	95.12	54.82	54.16	54.71	82.96	14.76	117.6
M649L[C]	22.92	82.01	38.01	68.54	73.58	72.83	47.07	28.83	96.72	41.98	62.24	55.8	175.5
M649T[E]	43.61	72.15	47.2	66.99	84	82.72	17.65	23.53	105.5	97.45	67.32	50.67	171.8
A662E[E]	100.1	101.7	51.92	83.82	132.1	129.6	69.05	44.16	134.3	110.9	70.83	37.18	183.2
T670L[C]	75.25	75.14	21.15	52.09	109.1	118.3	56.69	71.4	151.6	64.69	59.74	88.44	174.2
L693P[E]	88.03	73.82	86.89	88.84	96.19	107.3	83.23	39.29	93.76	111.5	63.13	71.82	169.4
M695T[E]	79.44	55.82	89.55	103.1	92.69	45.96	61.88	79.04	60.96	103.9	68.95	92.96	139.8
L699M[E]	55.85	69.13	57.75	89.07	90.94	42.28	60.88	69.08	90.47	90.9	66	51.01	134.2
A700T[C]	69.86	79.3	43.85	78.75	90.92	132.3	59.37	45.64	106.9	99.82	83.75	61.3	151.5
WT-CDC1551	136.2	93.86	114	129.8	159	150.7	96.38	151.5	148.2	154.7	123	97.66	193.8
Average WT - Erdman	115.96	74.87	101.18	115.1	142.74	140.3	89.33	141.14	130.32	138.96	94.88	69.12	171.88

E or C indicates the WT background that the AUC was compared to. E – Erdman and C – CDC1551